NANO · MICRO small
www.small-journal.com

Nanomaterials in 4D Printing: Expanding the Frontiers of Advanced Manufacturing

*Shengbo Guo, Haitao Cui, Tarun Agarwal, and Lijie Grace Zhang**

As an innovative technology, four-dimentional (4D) printing is built upon the principles of three-dimentional (3D) printing with an additional dimension: time. While traditional 3D printing creates static objects, 4D printing generates "responsive 3D printed structures", enabling them to transform or self-assemble in response to external stimuli. Due to the dynamic nature, 4D printing has demonstrated tremendous potential in a range of industries, encompassing aerospace, healthcare, and intelligent devices. Nanotechnology has gained considerable attention owing to the exceptional properties and functions of nanomaterials. Incorporating nanomaterials into an intelligent matrix enhances the physiochemical properties of 4D printed constructs, introducing novel functions. This review provides a comprehensive overview of current applications of nanomaterials in 4D printing, exploring their synergistic potential to create dynamic and responsive structures. Nanomaterials play diverse roles as rheology modifiers, mechanical enhancers, function introducers, and more. The overarching goal of this review is to inspire researchers to delve into the vast potential of nanomaterial-enabled 4D printing, propelling advancements in this rapidly evolving field.

1. Introduction

Since the inception of the first patent for 3D printing or additive manufacturing (AM) over four decades ago, this remarkable innovation has gained widespread adoption across various industries.[1–3] However, the static nature of 3D printing poses challenges in meeting the dynamic demands of specialized areas. Under such a background, the concept of 4D printing was initially presented in the 2013 TED Talk.[4] By adding "time" as the fourth dimension, 4D printing is defined as the transformation of a 3D-printed object's structure, property, and function following a preprogrammed procedure in response to external stimuli, such as temperature, light, or other environmental factors. Shape-changing behavior triggered by external stimuli has played a prominent role in the evolution of organisms, exemplified by the sunflower's ability to adjust its head to track the sun's position for optimal growth and reproduction.[5] Despite being a relatively novel technology, 4D printing has drawn substantial attention from academia and industries, with a diverse range of applications being explored, including but not limited to actuators, soft robotics, biomedical devices, and drug delivery systems.[6–9]

In 4D printing, the key distinction from traditional 3D printing arises from the utilization of smart materials in the printing process. Smart materials refer to materials that have the ability to respond to external stimuli by changing their properties or shape over time.[10] Smart polymers are favored in 4D printing over smart alloys and ceramics because of their printability, diverse responsiveness to stimuli, and substantial deformability. Whereas numerous functional materials can directly respond to external stimuli, various shortcomings, such as poor printability and insufficient deformation ability, still limit their application in 4D printing. In this case, the importance of material modification becomes highlighted. To develop 4D materials for various applications, researchers have explored various methods and achieved promising results, including but not limited to the incorporation of nano- or micro-materials, utilization of multiple materials, chemical modification, and manipulation of manufacturing processes.[11–15] Among those strategies, the introduction of nanomaterials is one of the most straightforward and efficient approaches.

Nanomaterials refer to materials that are characterized by at least one dimension on the nanometer scale, typically ranging

S. Guo, T. Agarwal, L. G. Zhang
Department of Mechanical and Aerospace Engineering
The George Washington University
Washington, DC 20052, USA
E-mail: lgzhang@gwu.edu
H. Cui
Key Laboratory of Biorheological Science and Technology
Ministry of Education
College of Bioengineering
Chongqing University
Chongqing 400044, China
L. G. Zhang
Department of Electrical Engineering
The George Washington University
Washington, DC 20052, USA
L. G. Zhang
Department of Biomedical Engineering
The George Washington University
Washington, DC 20052, USA
L. G. Zhang
Department of Medicine
The George Washington University
Washington, DC 20052, USA

The ORCID identification number(s) for the author(s) of this article can be found under https://doi.org/10.1002/smll.202307750

DOI: 10.1002/smll.202307750

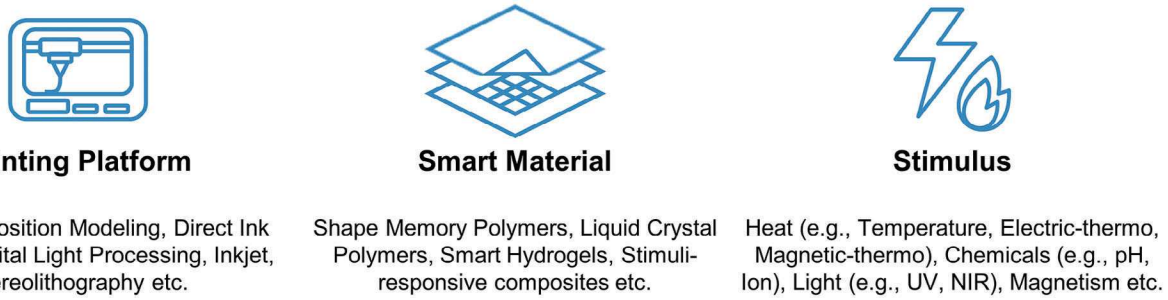

Figure 1. Schematic of three fundamental factors comprising 4D printing. 1) Printing platforms: Fused deposition modeling (FDM), direct-ink writing (DIW), digital light processing (DLP), stereolithography (SLA), inkjet printing, and others; 2) Smart materials: Shape memory polymers (SMPs), liquid crystal polymers (LCPs), smart hydrogels, shape memory alloys (SMAs), shape memory ceramics (SMCs), and stimuli-responsive composites; 3) External stimuli: Heat (e.g., temperature, electric-thermo, magnetic-thermo), chemicals (e.g., pH, ion), light (e.g., ultraviolet (UV), near-infrared light (NIR)), magnetism, and others.

from 1 to 100 nanometers.[16,17] At this scale, materials often exhibit unique and distinctive properties compared to their bulk or micro counterparts, and their unique properties can be primarily attributed to two factors: surface effects and quantum effects, which we will be discussing in more detail in later sections. These factors result in nanomaterials displaying improved or novel properties in terms of mechanics, thermal conductivity, magnetism, electronics, optics, and catalysis.[18] For example, gold nanoparticles (AuNPs), which are the nano-spherical form of gold, exhibit unique properties including but not limited to size- and shape- dependent optoelectronic properties, a large surface-to-volume ratio, outstanding biocompatibility, and minimal toxicity.[19–22] AuNPs have been extensively studied across various applications, including electronic devices and electrochemical sensing owing to their redox activity, colorimetric sensing, and photothermal therapy facilitated by their surface plasmon resonance (SPR), and imaging and sensing through their surface-enhanced Raman scattering (SERS).[23–28] In 4D printing, the function of nanomaterials can be summarized as modifiers of rheology, enhancers of mechanical properties, and contributors to the introduction of multiple functionalities. In this review, we begin by briefing technological considerations related to 4D printing. We then discuss the various nanomaterials that facilitate the functional behavior of 4D materials. Finally, we highlight the challenges faced in the field and present a glimpse into further prospects.

2. 4D Printing

While implementing 4D printing, several essential factors inherent to 4D printing should be taken into consideration. However, as a relatively new technology, there is no consistent summary of the components comprising 4D printing, primarily due to differing understanding of it.[29–32] In this review, we have summarized the key technological factors that constitute 4D printing, namely the printing platform, smart material, and stimuli, as illustrated in **Figure 1**, which will be discussed in more detail in the subsequent section.

2.1. Printing Platform

4D printing, as an extension of 3D printing technology, shares the same printing platform or technique as 3D printing. According to the ISO/ASTM 52 900 standard, AM is classified into seven categories: binder jetting, directed energy deposition, material extrusion, material jetting, powder bed fusion, sheet lamination, and vat polymerization.[33] Regarding 4D fabrication, the most commonly used techniques include material extrusion- and vat polymerization-based printing, as well as material jetting (**Table 1**).[31]

Extrusion-based printing systems, represented by fused deposition modeling (FDM) and direct-ink writing (DIW), stand out as one of the most extensively used and well-established printing techniques in 4D printing.[34–36] FDM platforms primarily utilize the transitions between solid and semi-molten states of thermoplastic polymers, followed by re-solidification, to facilitate layer-by-layer deposition in the printing process, thereby enabling the creation of 3D objects.[36–40] In FDM 4D printing study, many materials have demonstrated both direct or indirect thermoplasticity, along with shape memory properties, such as bisphenol A epoxy with benzoxazine, polycyclooctene (PCO) and a zinc-neutralized poly (ethylene-co-methacrylic acid).[29,41,42] However, polylactic acid (PLA) is more widely investigated and commercialized due to its easy accessibility, and it has been approved by the FDA for several biomedical applications owing to its low toxicity and biodegradability.[43,44] However, the requirements for thermoplastic material and the high temperatures generated during the printing process have largely limited the use of FDM printing in 4D printing. In contrast, DIW printing offers greater material versatility, including hydrogels, shape memory polymers (SMPs), and even multiple materials.[45–47] The fundamental principle of DIW is similar to FDM, but it involves pneumatic extrusion of viscoelastic inks. To maintain printing fidelity, the inks have to meet certain rheological requirements: 1) shear-thinning behavior (viscosity decreases when shear stress is applied), 2) consistent filament flow during extrusion, and 3) retaining more than 80% of the original viscosity after deposition.[48] In this regard, thixotropic agents are frequently employed to modify the rheological properties of inks in DIW printing, consequently enhancing printability.

A vat polymerization-based printing system, exemplified by stereolithography (SLA) and digital light processing (DLP), represents another commonly used technology in 4D printing. Different from extrusion-based printing, vat polymerization cures photo-cross-linkable resin into solid or semi-sloid constructs using a light-assisted system.[29,49] SLA is a well-established 3D

Table 1. Commonly used printing platform for 4D printing. Adapted with permission.[29] Copyright 1999–2023, John Wiley & Sons.

Printing Platform	Scheme and Primary Component	Features	Resolution	Typical Material in 4D Printing
FDM	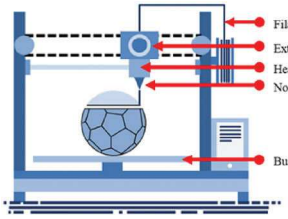	Line-by-line; Force-driven deposition of thermoplastic layers	X-Y Plane: 0.1 – 0.4 mm Z Direction: 0.5 – 0.127 mm	Thermoplastics, e.g., PLA,[66] and composites, e.g., PLA/PCL,[67] carbon black/PLA,[68] and Fe_3O_4 NPs/PLA[69]
DIW	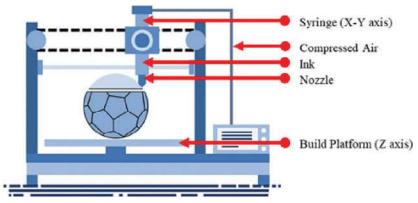	Line-by-line; Pressure-driven deposition of viscous ink through nozzle	X-Y Plane: ≈0.1 mm Z Direction: <100 µm	Hydrogels,[70] LCEs,[71] SMPs and multi-material[47]
SLA	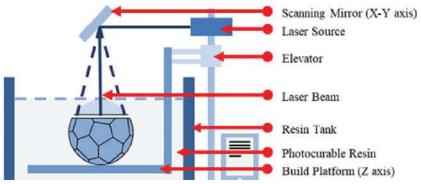	Dot-by-dot; Photocurable polymer solution is cured by laser beam	X-Y Plane: 25 – 300 µm Z Direction: 0.05 – 0.015 mm	Photocurable resins,[56,72] hydrogels,[73] LCEs, multi-materials[59]
DLP	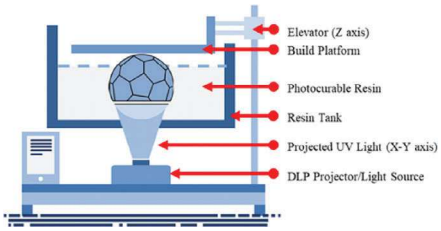	Face-by-face; Photocurable polymer solution is cured by projection	X-Y Plane: 0.6 – 200 µm Z Direction: 0.1 mm	Same as SLA printing
Inkjet	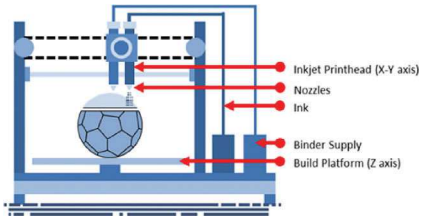	Drop-by-drop; Low viscosity inks deposited as droplets	X-Y Plane: 1 µm Z Direction: ≈2 µm	Hydrogels, e.g., GelMA/Gel-COOH-MA[62]
TPP	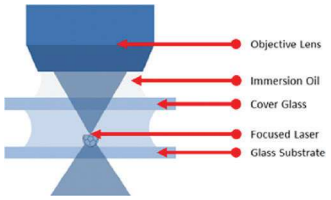	Dot-by-dot; Photocurable polymer solution is cured by focused femtosecond laser beam	X-Y Plane: 80–160 nm Z Direction: 100 nm	Photocuring resins, hydrogels,[74] LCEs[75]
PµSL	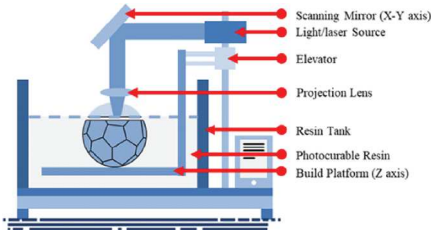	Face-by-face; Photocurable polymer solution is cured by projection	X-Y Plane: 0.6–30 µm Z Direction: 0.1 µm	Photocuring resins, SMPs,[76] hydrogel,[77] PEGDA[78]

DIW: Direct-ink writing; DLP: Digital light processing; FDM: Fused deposition modeling; Gel-COOH-MA: GelMA modified with additional carboxyl groups (–COOH); GelMA: Gelatin methacrylate; LCEs: Liquid crystal elastomers; PCL: Polycaprolactone; PEGDA: poly (ethylene glycol) diacrylate; PLA: Polylactic acid; PµSL: Projection micro stereolithography; TPP: Two-photon polymerization.

printing technique that uses laser emissions with varying wavelengths to initiate the photo-cross-linking process of photosensitive resins, ultimately forming the desired structures.[50] Thanks to the laser beam's fine focal point, SLA can achieve a resolution as fine as 25 µm.[51] Nevertheless, this resolution results in longer printing time, primarily owing to SLA's dot-to-dot printing manner.[52] In contrast, DLP platform allows to achieve higher printing speed through surface-projection-based fabrication, printing constructs in a layer-by-layer fashion. Moreover, DLP allows to achieve a better resolution compared to SLA.[53] Although SLA and DLP printing can attain superior resolution, their printing processes are complex and dynamic, meaning that even slight adjustment in printing parameters (for example curing time, layer height and laser/light intensity) can affect the quality or properties of the printed constructs, such as swelling ratios, inner stresses, and mechanical features.[54–56] Theoretically, any photocurable resin can potentially be printed using the SLA and DLP printing platforms, providing a wide range of material choices for 4D printing, including but not limited to photocurable hydrogels, photo-cross-linkable SMPs and liquid crystal polymers (LCPs), and even multi-materials.[15,57–59]

Material jetting, on the other hand, is relatively lesser-explored strategy for developing 4D printed constructs.[60] The technology is inspired by commercial inkjet printers and involves generating material droplets and depositing them onto a build platform under digital control to produce a 3D object.[60] It offers high resolution and multi-material printability, without requiring demanding printing condition like high temperature for nozzle in FDM printing.[61] In particular, materials with low viscosity are compatible with this technology, including, such as hydrogel, polymer, and even living cells.[62–64] However, major issues associated with it include low structural integrity and mechanical strength, nozzle clogging, and irregular droplet size and directionality.[65]

Despite SLA and DLP printing already achieving micron-level resolution, the pursuit of even higher-resolution printing persists, with extensive investigation currently underway in the field of 4D printing.[79–82] Direct laser writing (DLW) through multi-photon polymerization (MPP) is an advanced 3D printing method similar to SLA that uses laser scanning.[83] It can achieve a resolution even finer than 100 nanometers.[84,85] Typically, MPP technology relies on non-linear absorption, wherein two or more photons are simultaneously absorbed. This process enables localized polymerization in small volumes, referred to as "voxels," within a photosensitive resin, where the ultra-fast laser beam is precisely focused.[86] As a well-established form of MPP, two-photon polymerization (TPP) relies on the two-photon absorption (TPA) principle, in which a photosensitive molecule simultaneously absorbs two photons, transitioning from the ground state to an excited state, and thus initiating polymerization.[87] However, there are certain limitations to this technology, such as the requirement for high-intensity femtosecond laser pulses, typically ≈1 TW cm^{-2}, and the general limitation of printing volumes to the millimeter scale.[84,88] Similar to DLP or considered a variant thereof, projection micro-stereolithography (PµSL) cures photosensitive resin layer by layer, achieving resolutions of up to 600 nm through the use of the high-precision digital micromirror device (DMD).[89,90] These high-end printing technologies also enables versatile enhancement of 4D printing by controlling the material properties at feature sizes or spatial scales, which can reach to nanometer dimensions.[82,91–96]

2.2. Smart Materials and Stimuli

As stated previously, the process involved in 4D manufacturing primarily relies on established 3D printing technologies. What set 4D printing apart from conventional AM is the use of smart materials, also referred 4D materials or stimuli-responsive materials (SRMs). These materials are capable of altering their shape, properties, or functions in response to applied external stimuli, including but not limited to temperature, light, chemicals, magnetic fields, and electric fields.[10] The choice of stimuli highly depends on the material used in the printing process, the desired properties of the printed object, and the intended applications.[12,97,98] The mechanisms by which these stimuli can induce 4D effects are summarized in **Table 2**. In terms of shape-shifting, the 4D printed constructs can possess either shape memory or shape morphing capabilities in response to specific stimuli.[99–101] Shape morphing effect refers to an irreversible transition of an as-printed structure to another shape upon exposure to a specific stimulus, while the shape memory effects (SMEs) involves initial programming step and followed by recovery step.[31,102] The programming step involves deforming the structure to the original or permanent shape by subjecting it to a temperature higher than its glass transition temperature (T_g) and subsequently quenching it to form a metastable temporary shape, often referred to as fixation. Then, with an appropriate stimulus, the structure with the temporary shape will recover to the original shape, a step known as recovery. In this process, some key parameters are usually used to quantitatively measure the SMEs, for example, shape-fixation ratio (R_f), shape-recovery ratio (R_r) and shape-recovery rate (V_r), which quantify the ability of the SMPs to fix the temporary shape, recover to its original shape and the speed of recovery, respectively.[103] As illustrated in **Figure 2**, R_f, R_r, and V_r can be expressed using angle measurement as:[104]

$$R_f = \frac{\theta_{\text{Fixed}}}{\theta_{\text{Max}}} \times 100 \quad (1)$$

$$R_r = \frac{\theta_{\text{Fixed}} - \theta_{\text{Final}}}{\theta_{\text{Fixed}}} \times 100 \quad (2)$$

$$V_r = \frac{R_r}{T} \quad (3)$$

Currently, the smart SRMs engaged in 4D printing includes shape memory alloys (SMAs), shape memory ceramics (SMCs),SMPs, LCPs, stimulus-responsive hydrogels (SRHs), and stimulus-responsive composites (SRCs).[12,117–121] The processing of SMAs and SMCs often requires extremely high temperatures and pressures.[122,123] For example, a post-processing step is required to cure NiMnGa SMAs parts printed by metal binder jetting, which requires exposure to 1353 °C for 10 h in an argon atmosphere.[124] In contrast, polymeric SRMs such as SMPs, LCPs, and SRHs, offer ease of manufacturing using standard processing technologies. DIW (or FDM) printing is utilized for extruding liquid (or fused) polymeric materials with specific

Table 2. Different stimuli employed for 4D printing technology. Adapted with permission.[31] Copyright 2021, The Royal Society of Chemistry.

Stimuli	Mechanism of Action	Relevant Examples
Temperature	– Temperature-induced changes in material crystallinity, swelling	– PU[105] – PLA[106] – SOEA[107] – PS[108]
Light	– Photothermal effects	– SMMs containing photothermal agent (e.g., graphene, AuNPs)[12,71,109]
Magnetic Field	– Magnetothermal effect – Magnetic drive/actuation	– SMMs containing MNPs or magnetizable microparticle (e.g., Fe_3O_4 NPs, and NdFeB microparticles)[11,97]
Electric Current	– Electrothermal effects – Electric drive/actuation	– SMMs containing electroactive materials (e.g., PPy)/nanomaterials (e.g., MWCNTs, and AgNWs)/ionic liquid[110–113]
Chemicals	– pH-dependent variation in electrostatic interaction – Hydration induced swelling ratio difference – Desolvation induced differential volume compression due to cross-linking density gradient	– β-CD-Alg and DETA-Alg[114] – Nanocellulose incorporated hydrogel composite[115] – SLA printed SOEA with cross-linking gradients[57] – PEGDA in water/acetone system[116]

Alg: Alginate; AgNWs: Silver nanowires; AuNPs: Gold NPs; DETA: Diethylenetriamine; MNPs: Magnetic NPs; MWCNTs: Multi-walled carbon nanotubes; PPy: Polypyrrole; PS: Polystyrene; PU: Polyurethane; SMMs: Shape memory materials; SOEA: Soybean oil epoxidized acrylate; β-CD: β-cyclodextrin.

rheological properties, while DLP (or SLA) printing is theoretically suitable for all photo-cross-linkable materials. Taking PLA as an example, which is a thermoplastic SMP widely used for FDM printing, the typical printing temperature ranges from 180 to 220 °C, with some recommendations starting ≈200 °C and then adjusting as needed. A detailed description of different SRMs is beyond the scope of this review. Readers can refer to various previously published works to develop a better understanding of these topics.[29,125,126] We will primarily focus on an emerging category of 4D materials, namely stimuli-responsive nanocomposites (SRNcs), which involves utilizing nanomaterials as a component of 4D inks, expanding the opportunities for developing smart constructs for multifaceted applications.

3. Stimuli-Responsive Nanocomposites

In 4D printing, many functional materials possess the ability to respond to external stimuli, but their applicability is limited by a variety of constraints. For example, certain epoxy-based SMPs exhibit considerable SMEs; yet, they fail to hold the proper form after being extruded through the nozzle, suggesting poor printability. Moreover, given that the most of SMPs are thermo-responsive, actuating them in low-temperature environment is impractical. In such scenarios, non-thermal actuation methods such as photo-, magnetic-, or electric-actuation offers a solution by bypassing the necessity for temperature control to achieve 4D performance. To address such problems, considerable efforts have been dedicated, including but not limited to designing bi-/multi-layer structures, creating programmed patterns, and introducing multiple or functional materials. Among these strategies, the introduction of nanomaterials into the 4D material matrix has been most promising strategy.[127–129] Nanomaterials are generally characterized by their tiny size, with at least one dimension measuring less than 100 nanometers.[130] In terms of the dimensions of nanomaterials, they can be classified into zero, one, two, and three dimensions (0, 1, 2, and 3D), as shown in **Figure 3**.[131] At the nanometer scale, nanomaterials demonstrate unique or enhanced physical and chemical properties as compared to their macroscopic counterparts, mainly resulting from surface effects and quantum effects.[18,132] Thus, upon addition to the printing inks, nanomaterials can bring abought significant modulations in ink's mechanical, rheological, and functional performances. For instance, the low modulus of SMPs presents a significant drawback in various biomedical application, as a mismatch between a medical implant and the host tissue could potentially lead to implant failure. To overcome it, incorporating

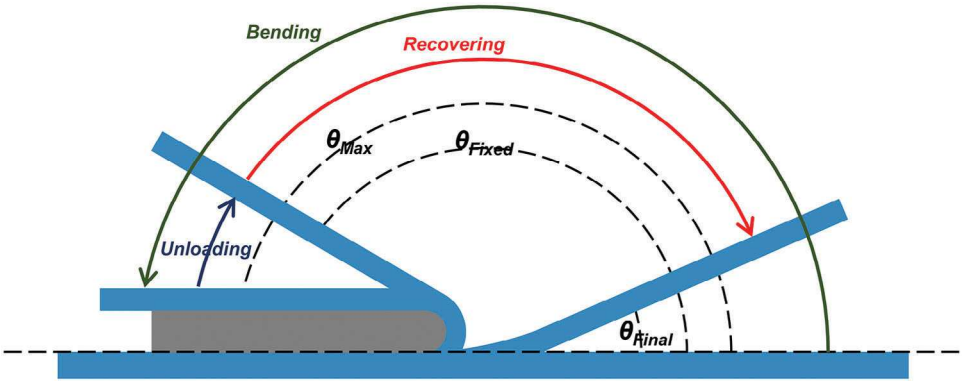

Figure 2. Schematic representation of angle measurement of 4D performance using a U-shaped sample.

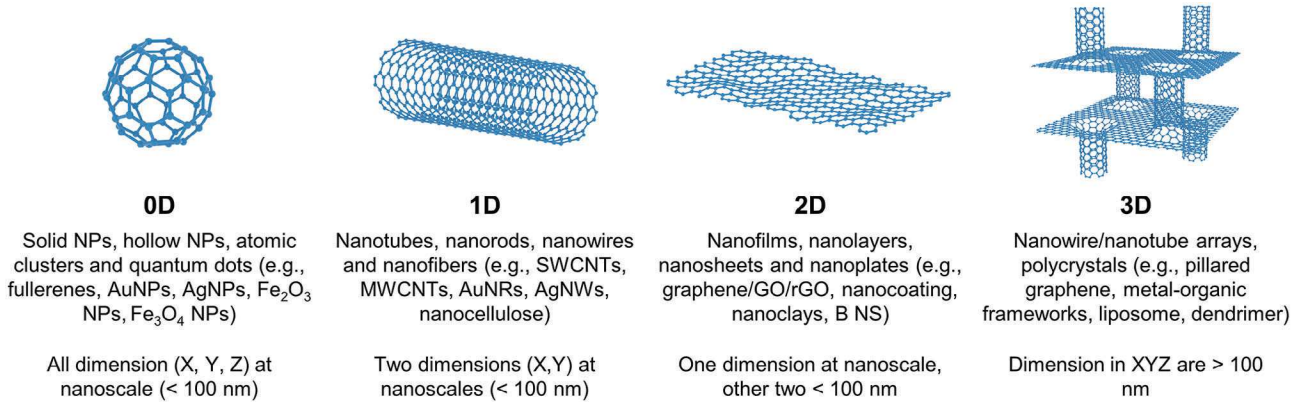

Figure 3. Schematic of the classification of nanomaterials according to their dimensions. AgNWs: Silver nanowires; AuNPs: Gold nanoparticles; AuNRs: Gold nanorods; B NS: Boron nanosheets; GO: Graphene oxide; MWCNTs: Multi-walled carbon nanotubes; rGO: Reduced graphene oxide; SWCNTs: Single-wall carbon nanotubes.

reinforcing nanofibers into printed constructs is being investigated widely to tune their mechanical properties. In addition, some materials possess unique properties that are well-suited for certain applications, yet their rheological properties make them unprintable. The addition of nanomaterials can allow us to overcome this challenge. Moreover, although some materials possess SMEs, the 4D performance is limited, for instance, a low recovery rate. Under such a condition, the incorporation of nanomaterial is able to amplify the 4D performance of the 4D printed structures. Last but not least, the introduction of nanomaterials can introduce new functionalities into 4D constructs. For example, by doping graphene nanoplates (GNPs) into thermo-responsive SMPs, the photothermal-responsive ability could be introduced, expanding their potential application.[12] In the following section, we present a comprehensive overview, with a particular focus on the utilization of nanomaterials in 4D printing.

3.1. Nanomaterials as Rheology Modifiers

As mentioned previously, a wide spectrum of functional materials, with the capacity to respond to external stimuli, possesses the potential to actuate desired 4D effects. Despite their potential, the comprehensive utility of these materials in 4D printing is hindered by limited printability, such as inappropriate rheological properties, demanding curing conditions, and slow curing rate.[133] For example, thermoset epoxies and their composites are promising candidates as SMPs, demonstrating the thermoresponsive SMEs.[134] However, most of epoxy materials are derived from liquid-based resins containing epoxide groups in which form the ink cannot maintain a proper shape after being extruded through a fine nozzle due to the lower viscosity. In addition, epoxy is a thermally cured material, requiring specific cross-linkers, high temperatures, and an extended duration for the curing process, rendering it unsuitable for direct 4D printing using DIW.[135] Due to the properties of epoxy-based materials, cast molding is the most commonly used method for their fabrication but imposes restrictions on the design of intricate geometries. In this regard, the introduction of nanomaterials has been extensively investigated as a promising strategy, rendering them suitable for extrusion-based printing by modulating their rheological characteristics (**Table 3**). DIW printing is often the preferred option due to its excellent printing material versatility.[136] But the ink for DIW printing is required to possess adequate yield stress and shear-thinning behavior, ensuring easy extrusion through nozzles while quickly recovering to high viscosity and elastic behavior to retain its shape after deposition.[137–139] In particular, the ink's rheological behavior should demonstrate a relatively high viscosity, which rapidly decreases under shear force and promptly reverts to its initial viscosity upon the cessation of shear force. This characteristic enables the ink to smoothly pass through fine nozzles and stack on substrates or previously printed layers without spreading or collapsing. The mathematical representation of the shear stress (τ) of the inks can be described by the Herschel-Bulkley model:[140,141]

$$\tau = \tau_Y + K\dot{\gamma}^n \quad (4)$$

where τ_Y is the yield stress, K is the flow consistency index, $\dot{\gamma}$ is the shear rate, and n is the flow index ($n < 1$ for shear-thinning fluids), respectively.[140] Generally, for inks to flow through the nozzle during printing, the applied shear stress τ must exceed the τ_Y of inks; once extruded, τ of the inks should quickly recover to their original τ_Y.[140] As such, the inks are extruded from the nozzle in a liquid form due to the shear thinning while retaining its original shape as a viscoelastic solid after extrusion.

As rheology modifiers, nanomaterials can modulate the rheological properties of composite inks through the increase of viscosity to enable the printing of complex architectures. They provide the composite inks with rheological behaviors, from viscoelastic for control of shape to pure Newtonian fluid for particle orientation.[142] Newtonian fluids demonstrate a constant viscosity while incorporating nanomaterials into a Newtonian fluid can induce non-Newtonian behaviors, such as shear thinning and shear thickening.[143] Assessed by experimental data fitting to flow curves, the Oswald de-Waele empirical model can be used to describe the rheological behavior of composite inks:[143,144]

$$\eta = K\dot{\gamma}^{-n} \quad (5)$$

where η is viscosity, and n is the power-law exponent. $n = 0$ designates a Newtonian fluid while $n > 0$ represents shear thinning

Table 3. Nanomaterials as rheology modifiers in 4D printing studies.

Nanomaterial	Nanomaterial Modification/ Treatment	Material	Printing Technique	Stimuli	Key Features Incorporated Due to the Addition of Nanomaterials	Refs.
Nanosilica	Acrylated Nanosilica	DEGDA, tBA, BAPO	DLP	Thermal	• Nanomaterial concentration: 2.5 wt.%. • Decrease in required layer exposure time from 4 s to 0.7 s for printing. • Tensile strength improvement: 2.4–3.6 times (v/s neat SMP). • Higher elongation at break: ≈4.7 times (v/s neat SMP) • Better shape memory life cycle: ≈2 times (v/s neat SMP)	[145]
	Physical Mixture	Rapid-curing System (Epon 826, ePB-h, Epikure 3140)/ Slow-curing System (Epon 826, ePB-h, Epikure W)	DIW	Thermal	• Nanomaterial concentration: 10 and 7 wt.% (rapid-curing system) and 13 wt.% (slow-curing system). • Allowed to achieve appropriate thixotropic rheology for printing.	[146]
	Physical Mixture	PU	DIW	Thermal	• Nanomaterial concentration: 8 wt.%. • Allowed to achieve appropriate thixotropic rheology for printing. • Reduction in fracture stain: ≈5.8 times (v/s pure PU). • Ultimate tensile strength improvement: ≈3.78 times (v/s pure PU).	[147]
	Physical Mixture	AUD/BA/PCL	DIW	Thermal	• Nanomaterial concentration: 4 wt.%. • Incorporating shear-thinning and shape fidelity effects to improve ink printability	[148]
	Physical Mixture	SE 1700, Ecoflex 00–30, NdFeB Microparticles	DIW	MF	• Nanomaterial concentration: 2.72 wt.%. • Improved mechanical properties, including shear thinning and shear yielding.	[11]
Nanoclays	Physical Mixture	BPADA, DABA, ODA, HEMA, Irgacure 2100, IBOMA, HQ	DLP/DIW	Thermal	• Nanomaterial concentration: 25 wt.%. • Improved shear thinning and storage modulus, improving ink printability.	[149]
GNPs	Physical Mixture	E51, MeHHPA, DMP-30	DIW	Thermal	• Nanomaterial concentration: 10 wt.%. • Improved shear thinning, yield stress, and storage modulus, improving ink printability	[150]

AUD: Aliphatic urethane diacrylate; BA: n-Butyl acrylate; BAPO: Phenylbis (2,4,6-trimethylbenzoyl) phosphine oxide; BPADA: 4,4′- (4,4′-Isopropylidenediphenoxy) diphthalic anhydride; DABA: 3.5-Diaminobenzoic acid; DEGDA: Di (ethylene glycol) diacrylate; DMP-30: Tris (dimethylaminomethyl) phenol; ePB-h: Epoxide-functionalized, hydroxyl-terminated polybutadiene; HEMA: β-Hydroxyethyl methacrylate; HQ: Hydroquinone; IBOMA: Isobornyl methacrylate; MeHHPA: Methylhexahydrophthalic anhydride; ODA: 4,4′-Diaiminodiphenyl ether; tBA: tert-Butyl acrylate.

fluid and $n < 0$ represents shear thickening fluid.[144] For DIW printing, the range between 10^2 and 10^6 mPa s ($\dot{\gamma} \approx 0.1\ s^{-1}$) is highly recommended to ensure the printability of the inks.[140] Aspect ratio and volume fraction of nanomaterials and intrinsic viscosity of inks are considered the important variable that significantly influence the rheology of composite inks. Taking nanocellulose as an example, the relationship between aspect ratio and intrinsic viscosity is established for highly dilute suspensions of elongated particles as:[143,144]

$$[\eta] = \frac{4}{15}\frac{r^2}{\ln r} \tag{6}$$

where r denotes the aspect ratio (the length-to-diameter ratio). In the dilute condition, hydrodynamic forces and particle-particle interaction are negligible.[143] However, when a higher concentration of NPs is incorporated, the equation can be expressed as:[143,144]

$$\eta/\eta_0 = 1 + \frac{\pi}{90\ln r}\nu L^3 + \frac{\pi}{30\beta\ln r}\left(\nu L^3\right)^2 \tag{7}$$

where L represents the scale length, v stands for the number density of rods, and β is the measure of freedom degree among particles.[144] When a non-entanglement model is applied, the equation can be modified:[143,144]

$$\eta/\eta_0 = 1 + \frac{\pi}{90\ln r}\nu L^3 + \frac{\pi}{30\beta\ln r} \times \left[1 + \frac{\nu L^3}{\sqrt{\beta}(1-\varepsilon \mathrm{v} D L^2)}\right]^2 \nu L^3 \tag{8}$$

where D represents the rotational diffusion coefficient. Moreover, the affinity of nanomaterials for ink materials is determined by the interface interaction between them, e.g., hydrophobic, and hydrophilic properties, electrostatic force, hydrogen bond, and supramolecular interaction, leading to the difference of viscosity change for the use of different nanomaterials. Although there are still few studies about the rheological properties of various nanomaterials in inks, these theoretical models in composite systems could help us explore the effects of nanomaterials on the rheological behaviors of 4D inks.

Silica NPs, commonly referred to as fumed silicas, are one of the most frequently used inorganic rheology modifiers that comprise finely dispersed amorphous silicon dioxides with diameters ranging from 5 to 50 nm.[151,152] Characterized by highly reactive silanol (Si-OH) groups on surface, fumed silica is capable of forming hydrogen bonds among themselves and with the surrounding matrix, resulting in reversible agglomeration that manifests macroscopically as thickening.[153,154] As it is reversible, stressing the inks reveres the agglomeration, making it more fluid and reducing viscosity. It is then restored to its original value when the system is at rest and the interaction rebuilds. This phenomenon is referred to as thixotropy.[155,156] By incorporating fumed silica, Su et al. fabricated a PU nanocomposite with proper viscoelastic characteristics that could be printed using a homemade DIW printing device, as illustrated in **Figure 4a**.[147] In comparison to pure PU, the nanocomposite containing fumed silica within the range of 6–10 wt.% showcased favorable rheological properties. To elaborate, the PU nanocomposite with 8 wt.% fumed silica demonstrated solid-like behavior in low-stress situations, while the material transitions to a liquid-like behavior over a shear stress of 139 Pa. In addition, fumed silica also improved printing resolution and additive manufacturability without alternating their SMEs (Figure 4b,c). Chen et al. developed two systems for 4D printing commercial epoxy-based resins – Epon 826 with the fast-curing cross-linker Epikure 3140 (cyclo-aliphatic-based) and the slow-curing cross-linker Epikure W (aromatic-based), respectively (Figure 4d).[146] Addition of silica NPs (7–10%) significantly improved the printability of inks. As illustrated in Figure 4e, the printed structure demonstrated shape memory behavior upon heating. In another study, Kim et al. developed an innovative nanocomposite ink to fabricate magnetically-actuable 4D-printed constructs (Figure 4f,g).[11] The inks consisted of silicone rubber matrix, along with Nd–Fe–B microparticles (62.62 wt.%) and fumed silica NPs (2.72 wt.%) that imparted magnetic responsiveness and improved their printability. Interestingly, using an external MF mounted around the orifice, the embedded ferromagnetic microparticles may be controlled and redirected, creating domain patterns with varied magnetic pole directionalities. Such printed structures were capable of undergoing complex structural transformations under applied MF, depending factors like domain patterns, MF strength, and actuation fields. Apart from its application in DIW printing, fumed silica is also capable of manipulating the curing rate of photocurable resin.

Nanoclays, layered mineral particles ranging in size from ≈100 nm to a few microns, can be classified into various classes – montmorillonite (Mt), bentonite, kaolinite, hectorite, and halloysite – according to their chemical composition and morphology.[157] Li et al. modified the rheological properties of a photo-cross-linkable polyimide resin using nanoclays, transforming it into a DIW printable material (Figure 4h).[149] As expected, the addition of 25 wt.% nanoclays to the polymer matrix resulted in shear thinning and a high storage modulus, making the ink printable. However, the storage modulus remains lower than the loss modulus throughout the printing process, suggesting that the extruded ink tends to prefer fluidic leveling, which is not conducive to molding fidelity. To solve this issue, they set an in situ UV light to precisely cure the ink, thereby ensuring the preservation of morphology fidelity of the printed structures. Additionally, a smart gripper was fabricated using UV-assisted DIW printing, and upon thermal stimulus, the gripper successfully lifted a 4.05 g steel ball, as shown in Figure 4i.

GNP, a nanostructured carbon allotrope, is composed of a singular layer of carbon atoms arranged in a hexagonal lattice structure, where each atom is covalently bonded with three neighboring carbon atoms.[158] GNP is another widely investigated thixotropic agent due to its dispersing effect and the nanosheet alignment within the flowing plane, resulting in reduced viscous dissipation.[159,160] Chi et al. developed a DIW-printable and recyclable epoxy-based SMP nanocomposite (Figure 4j,k).[150] The introduction of GNP adjusted the rheological properties of the resin, and once the GNP content exceeded 7.5 wt.%, the storage modulus surpassed the loss modulus, resulting in their sol-gel transition. In addition, incorporation of GNPs also enhanced the thermal and electrical conductivity of the printed structure, thereby expanding its versatility and potential applicability.

3.2. Nanomaterials as 4D Mechanical Enhancers

In 4D printing, the mechanical properties of the printed materials dictate the performance, reliability, functionality, and compatibility of the printed structures. Moreover, inappropriate mechanical properties consistently limit their potential applications. For instance, in tissue engineering, a mechanical mismatch between a medical implant and the host tissue can induce a foreign body reaction, resulting in inflammation, fibrosis, and potential implant failure.[161,162] In 4D-printed soft robotics or actuators, the vital aspects of elasticity and flexibility enable shape morphing and adaptive responses, while the mechanical strength and durability of the printed materials ensure structural integrity and longevity. Additionally, properties like surface texture, adhesion, and friction coefficients influence object interaction and manipulation. In many cases, the inappropriate mechanical properties of the smart materials limit their application. To address this issue, the introduction of nanomaterials is being widely investigated and has emerged as a promising strategy (**Table 4**).

Most 4D polymeric materials typically exhibit relatively low elastic moduli, such as thermosets, where minor stress could induce brittle failure. However, composites that incorporate nanomaterials can withstand higher stress, demonstrating both elastic and plastic deformation before experiencing ductile failure.[163] There is abundant experimental evidence supporting the significant role of nanomaterials in enhancing the stiffness, strength, and toughness of polymer nanocomposites. Nanoscale reinforcements contribute to intrinsic toughness enhancement in polymer composites in two primary ways: 1) by increasing the plastic zone size, or 2) facilitating extrinsic toughness through

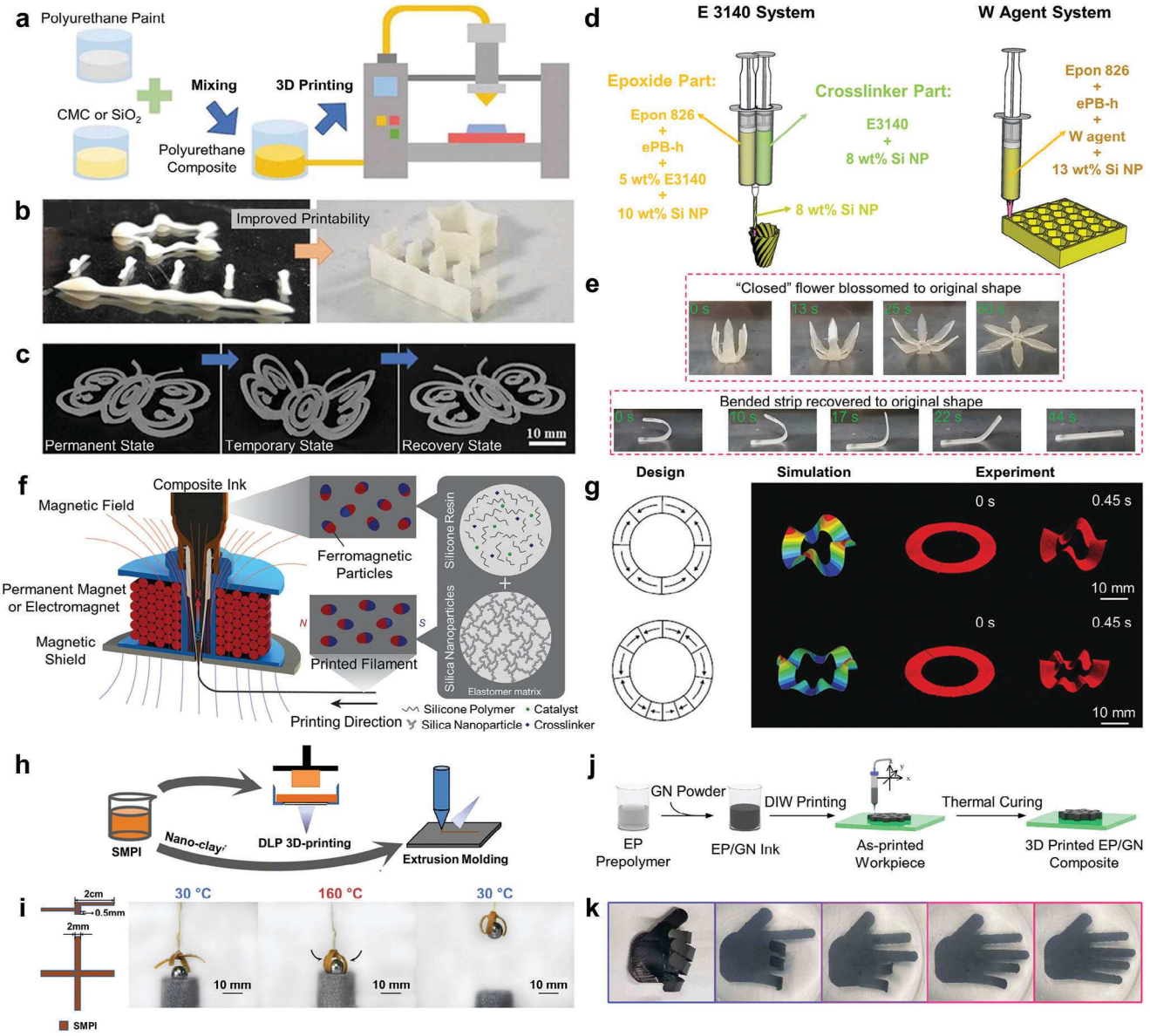

Figure 4. Nanomaterials as rheology modifiers. a–c) 4D DIW printing of silica NP modified PU-based composites. a) Schematic of the homemade 3D printing system for PU nanocomposites. b) The incorporation of silica NPs improved the printability of PU composite. c) The printed structure (butterfly pattern) of the nanocomposite exhibited the SME. Panels a–c are reprinted with permission.[147] Copyright 2023, Informa UK. d,e) A dual approach in DIW of silica NP modified shape memory epoxy. d) Schematic of the two different printing systems (E3140 and W agent) printing processes. e) The introduction of silica NPs made epoxy-based SMPs printable without alternating the SME of the printed structure. Panels d,e are reprinted with permission.[146] Copyright 2023, American Chemical Society. f,g) 4D printing of ferromagnetic domains for rapid transformation of untethered soft material. f) The orientation of the incorporated ferromagnetic microparticle can be navigated by an external permanent magnet or electromagnet while printing. g) Two programmable planar structures exhibiting complex shape-changing performance through applied MF and programmed ferromagnetic domains (design, simulation, and experiment). Panels f,g are reprinted with permission.[11] Copyright 2023, Springer Nature. h,i) Dual-method molding of 4D shape memory polyimide ink modified with nanoclays. h) The inclusion of nanoclays enabled the DIW printability of photocurable shape memory polyimide (SMPI) ink. i) DIW-printed gripper. Upon thermal stimulus, the gripper was able to lift a 4.05 g steel ball. Panels h,i are reprinted with permission.[149] Copyright 2023, Elsevier B.V. j,k) DIW printing of multifunctional composite composed of GNP-modified epoxy resin. j) Schematic of the preparation of DIW-printable 4D ink composed of GNPs and commercial epoxy resin. k) Shape memory performance illustrated using the 4D printed structure with a palm pattern. Panels j,k are reprinted with permission.[150] Copyright 2023, American Chemical Society.

Table 4. Nanomaterials as mechanical enhancers in 4D printing studies.

Nanomaterial	Nanomaterial Modification/Treatment	Material	Printing Technique	Stimuli	Key Features Incorporated Due to the Addition of Nanomaterials	References
GNPs	Physical Mixture	Epon 826, NGDE, Jeffamine D230	DIW	Thermal	• Nanomaterial concentration: 0.1 wt.%. • Tensile strength improvement: 30% (v/s neat SMP). • Elastic modulus improvement: 17% (v/s neat SMP). • Higher shape recovery rate: 16% (v/s neat SMP). • Better storage modulus: 356% (v/s neat SMP).	[175]
	Physical Mixture	SOEA	SLA	Thermal/ Chemical	• Nanomaterial concentration: 0.8 wt.%. • Causes higher laser attenuation, thereby creating higher laser-induced graded internal stress. • Decrease in printed stand thickness: ≈2.5 times (0.8% v/s 0.2% graphene-SMP) • Better shape curvature (v/s neat SMP).	[57]
Nanocellulose	Physical Mixture	PU	DIW	Thermal	• Nanomaterial concentration: 3 wt.%. • Decrease in T_g value: 34 °C (v/s 47 °C for neat SMP) • Tensile strength improvement: 71% (v/s neat SMP). • Allowed to achieve appropriate shear thinning properties for printing.	[176]
	Physical Mixture	DMAm/NIPAm, Laponite XLG Clay, Irgacure 2959, Glucose Oxidase, Glucose	DIW	Hydration	• Nanomaterial concentration: 0.78% (NCF) and 9.7% (Laponite XLG Clay). • Allowed to achieve appropriate shear thinning properties for printing.	[115]
	Physical Mixture	PCL/PBA	FDM	Thermal	• Nanomaterial concentration: 1 phr. • Tensile strength improvement: 25% (v/s neat SMP). • Higher elongation at break: 51% (v/s neat SMP) • Better shear thinning properties, improving its printability. • Better shape recovery time: ≈1.2 times (v/s neat SMP)	[177]

DMAm: N, N-dimethylacrylamide; Jeffamine D230: Poly (propylene glycol) bis(2-aminopropyl) ether; NGDE: Neopentyl glycol diglycidyl ether; NIPAm: N-isopropylacrylamide; PBA: Poly butylene adipate-co-terephthalate.

mechanisms like crack bridging and particle pull-out.[163] Nanocomposite, including interphase, interface, and change of a local morphology in the matrix, have a significant effect on intrinsic toughening, e.g., plasticity, molecular interlocking, viscoelasticity, and chain sliding.[163] Taking nanofibers for an example, the micromechanics of composites can be simply described by Young's modulus of a composite E_c:[164]

$$E_C = E_f\ V_f + E_m\left(1 - V_f\right) \tag{9}$$

where E_f and E_m are the moduli of the fiber and the matrix, and V_f is the volume fraction of the fiber.[164] When orientation, length (or aspect ratio), and agglomeration of the fibers are also considered, the equation can be modified:[164]

$$E_C = E_{ff}\ V_f \eta_o \eta_l + E_m\left(1 - V_f\right) \tag{10}$$

where E_{eff} represents the effective modulus of the fibers, η_o denotes the Krenchel orientation factor (the average orientation of the fibers in relation to the applied stress), and η_l is the length factor (fiber length and the interface length).[164] Continuum theories have widely been applied to explain micrometer damage; however, they are not able to capture nanoscale features.[163] Besides the interaction between NPs and polymer matrix,[165] the size, shape, stiffness, toughness, strength, concentration, and spatial organization of NPs are crucial factors in affecting the mechanical properties of composites.[164,166–168] However, their strengthening and toughening mechanisms for the polymeric matrix are not relatively clear. Some different mechanisms have been proposed, e.g., the Payne effect, immobilized polymer layer formation, hierarchical nature of chain-bound clusters, polymer bridges between NPs, and others.[167,169–173] Recently, some in situ characterization experiments, such as transmission electron microscope, scanning electron microscope, atomic force microscope, X-ray CT, piezo-resistive network, small-angle neutron

scattering, and Raman spectroscopy, have provided a reliable methodology to validate the multiscale failure mechanisms in nanocomposites through investigating the damage development at the NP/polymer interface under applied loading.[163,164,174] Additionally, in-depth mechanistic insights into the atomic-scale mechanical behavior of the polymer nanocomposites can be obtained through atomistic simulation, such as molecular dynamics simulation.[163,173,174] Although it is still unexplored that the mechanisms of nanomaterials serve as mechanical enhancers in 4D printing studies, these previous theoretical and experimental results are also suitable for our 4D polymeric nanocomposites.

As mentioned earlier, graphene is a monolayer of carbon atoms tightly bound in a hexagonal honeycomb lattice, enabling it to be an excellent mechanical enhancer for polymer reinforcement.[178] The introduction of graphene into the polymer matrix imparts remarkable stability and high tensile strength to the material, along with other unique properties. These include the ability to undergo larger deformations and recover more quickly when subjected to external stimuli.[179–181] This property is attributed to the covalent and/or non-covalent interaction between graphene and 4D matrix.[182] Covalent functionalization involves linking functional motifs (e.g., $–NH_n$, $–CH_n$, –OH, and –COOH) of the polymeric matrix to the carbon backbone of GNPs covalently, changing the hybridization from sp^2 to sp^3; meanwhile, the damage of the π-conjugation bond occurs. On the other hand, the non-covalent surface functionalization works by supramolecular chemistry, which includes π–π interactions, hydrophobic forces, hydrogen bonding, van der Waals forces, ionic bonding, and electrostatic effects between GNPs and the polymeric matrix. The same attributes are likewise evident in various modified forms of graphene, for instance, graphene oxide (GO) and reduced graphene oxide (rGO).[183,184] Thus, GNPs have been widely used as an important nanofiller in 4D printing. For example, using GNPs and SOEA, Miao et al. developed dual thermo- and mechano-responsive constructs through SLA-based printing (**Figure 5**a,b).[57] The presence of GNPs acted as photoabsorbers and control light penetration of laser through the ink, leading to laser-induced graded internal stress responsible for amplified 4D shape morphing. It was demonstrated that the GNPs content in SOEA significantly modulated the shape recovery response using a series of bird-flying architectures as illustrated in Figure 5c. In addition, a proof-of-concept smart nerve guidance conduit (NGC) was fabricated in the study for neural regeneration, as shown in Figure 5e,f. In another research, Idowu et al. synthesized a composite ink of epoxy-based SMPs with incorporated GNPs, which could be printed using a cryo-assisted extrusion printing system.[175] Besides the enhanced SME, the incorporation of GNPs also increased tensile strength and elastic modulus. The interaction between GNPs and the SMP creates a pathway that facilitates the transfer of stress and conduction of photons, resulting in an improvement in mechanical and thermal properties. Furthermore, the introduction of a moderate quantity of GNPs is able to enhance the surface roughness of the printed structure.[185]

Nanocellulose is a nanostructured form of cellulose derived from various sources such as wood, agricultural biomass, algae, and even bacteria.[186] Based on their morphologies, fabrication methods, and properties, nanocellulose is classified into three primary classes: 1) cellulose nanofibers (CNFs), 2) cellulose nanocrystals (CNCs), and 3) bacterial nanocellulose (BNC).[187] In addition to high mechanical strength, thermal stability, and aspect ratio, the hydroxyl groups of nanocellulose promote self-association, rendering it an effective reinforcing material in polymer composite matrices.[188,189] Furthermore, being a naturally derived nanomaterial, nanocellulose exhibits excellent biological properties, such as biocompatibility and biodegradability, which renders it an exceptionally promising biomaterial for a range of medical applications, including tissue engineering, wound dressing, and medical implants.[190] In a recent study, Gu et al. successfully incorporated CNFs as reinforcing fillers into thermo-responsive SMP composed of polycaprolactone/poly butyleneadipate-co-terephthalate (PCL/PBAT), creating a nanocomposite filament capable of being printed using the FDM printing (Figure 5g).[177] Owing to the bridging effect between CNFs and the polymeric matrix, the introduction of 1 part per hundred (1 phr) of CNFs significantly enhanced the mechanical performance, increasing the composite's strength from 14.72 to 18.53 MPa and elongation at break from 595% to 900% compared to the pure polymer.[191,192] However, when the CNFs content exceeds 1 phr, the mechanical performance of the nanocomposite decreased due to stress concentration induced by CNFs agglomeration within the composites' matrix, resulting in the formation of flaws and reduction in the mechanical characteristics of the composites.[193] Additionally, incorporating 1 phr CNFs does not affect the nanocomposite's shape fixation and recovery ratio, but it extends the recovery time. This phenomenon is attributed to the presence of CNFs as rigid particles, which affect the microscopic Brownian motion of the PCL phase by absorbing stored energy within the stationary phase and prolonging the contraction time of PCL molecular chains, as opposed to the neat SMP.[194] To demonstrate its potential in soft robotics and artificial muscles, they fabricated a bionic model capable of climbing plants in spiral curls in response to environmental stimuli and a bionic soft griper as illustrated in Figure 5h.

Inspired by botanical systems, Gladman et al. created a hydrogel nanocomposite ink with hydration-triggered swelling behavior.[115] As illustrated in Figure 5i, as the ink flows through the deposition nozzle, nanocellulose fibers undergo shear-induced alignment, enabling local control of cellulose orientation within the printed structure. In Figure 5j, significant cellulose fibril alignment was observed in contrast to isotropic casting. Through this method, the control of elastic and swelling anisotropies can be achieved, enabling the manipulation of the 4D performance of the printed constructs, as depicted in Figure 5k. CNFs were incorporated into a soft acrylamide matrix as stiff fillers. The internal alignment of CNFs within the composite could be manipulated by the printing pathway, as demonstrated in Figure 5i, allowing for control over the 4D morphing behavior through swelling anisotropies of CNFs (Figure 5j). In addition, the introduction of nanocellulose can also enhance the 4D effect of the printed structure. By adding an appropriate proportion of CNCs and ball-milled nanocelluloses, Zhou et al. fabricated a PU/nanocellulose nanocomposites with improved shape fixation ratio (R_f, >99%) and the shape recovery rate (R_r, >99%) compared to the pure PU.[176] Moreover, the nanocomposite demonstrated a tunable T_g associated with the nanocellulose content, enabling the preparation of printed structures with a T_g closely matching the human body temperature.

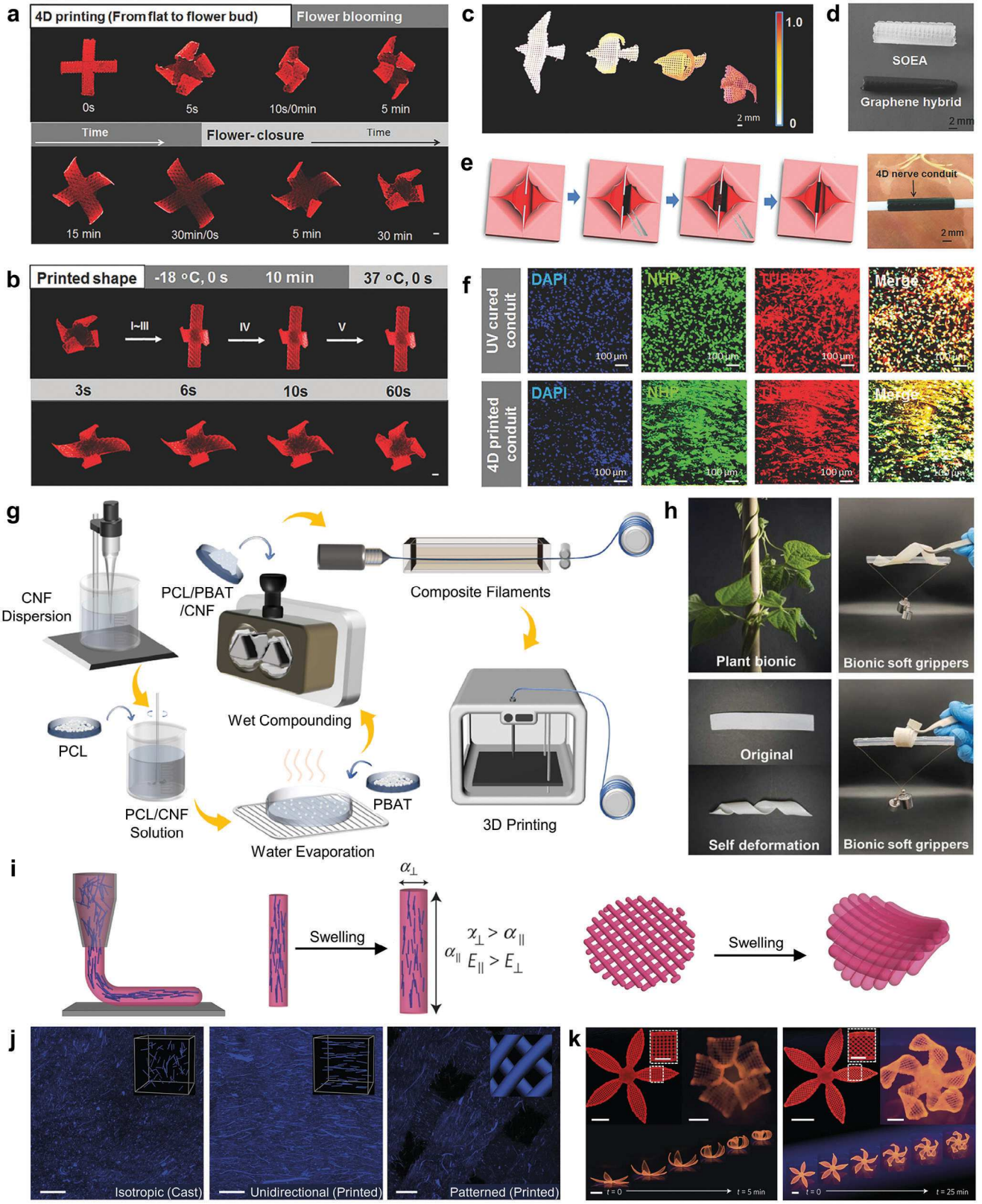

Figure 5. Nanomaterials as 4D mechanical enhancers. a–f) Stereolithographic 4D printing of GNPs enhanced SOEA. a) Thermo-responsive shape memory performance of SLA-printed SOEA structure. b) Chemical-responsive (ethanol) shape memory performance of SLA-printed SOEA structure. c) A sequence of bird-flying structures was generated using SOEA with increasing contents of GNP (from 0 to 0.8%). d) Illustration of the 4D reprogrammable NGC fabricated from SOEA without/with GNPs. e) Schematic of 4D nerve guidance conduit's shape transformation triggered by a thermal stimulus.

Given such physiochemical properties of nanocellulose, the fabricated nanocomposite could be potentially applied as smart 4D biomaterials.

3.3. Nanomaterials for Multifunction

Thermal actuation remains the most popular strategy for triggering the 4D effect, owing to the intrinsic thermo-responsive features of smart materials. More specifically, the underlying process of temperature-induced 4D actuation at the micro level involves the movement of molecules generated by heat within printed constructs, resulting in shape changes at the macro level.[195] However, direct heating methods like water bath or oil bath always require the constructs to directly contact the heat source, significantly limiting the application of 4D printed constructs in scenarios where direct thermal actuation is not feasible.[68,135] To address this issue, remote-actuated 4D constructs can be readily fabricated by incorporating stimulus-sensitive nanomaterials (e.g., photothermal, electrothermal, magnetothermal nanomaterials) into thermo-responsive SMP matrix, for instance, photothermal nanomaterial (e.g., GNPs, carbon nanotubes (CNTs), AuNPs, etc.), magnetic sensitive nanomaterial (e.g., Fe_3O_4 NPs, etc.) and conductive nanomaterial (e.g., AgNPs, AgNWs, etc.), which will be discussed in the following sections.

3.3.1. Nanomaterials as Photothermal Fillers

In 4D printing, photo-responsive materials are capable of undergoing deformation or shape recovery in response to light, including but not limited to visible light, near-infrared (NIR) light, and ultraviolet (UV) light.[12,196,197] Photo-responsive materials can be categorized into two classes according to their chemical compositions and mechanisms: photochemical- and photothermal-responsive materials.[12,198,199] Photochemical-responsive materials feature photo-chemically reactive functional groups, such as azobenzene and cinnamic groups, within polymer networks, and their reaction is initiated by light, thus triggering the shape-changing performance.[200,201] On the contrary, the incorporation of photothermal materials, majorly nanomaterials, has emerged as a more efficient and promising strategy for fabrication of photo-responsive 4D constructs (**Table 5**). Moreover, using light as a stimulus for 4D effect actuation offers advantages over direct heating-based approaches. For instance, light, particularly NIR, can serve as a potentially benign stimulus for the 4D actuation of the constructs, preventing potential tissue damage caused by heating or burning in biomedical applications.[201] By use of light sources with appropriately different wavelength, or localized illumination, more complex 4D performance can be realized. For example, by doping azobenzene and GO into SMP matrix, Zhou et al. fabricated a construct with two-stage 4D shape-changing performance that is actuated by UV and NIR light respectively.[109] In another study, Cui et al. utilized SMP doped with GNPs to fabricate a palm, enabling independent manipulation of each finger through partial illumination of NIR.[12]

Plasmonic nanomaterials, one of the most extensively investigated photothermal materials, demonstrate both strong and broad-spectrum absorption throughout the UV–visible–NIR region, enabling efficient conversion of light into heat by leveraging the phenomenon of localized surface plasmon resonance (LSPR).[208] Upon appropriate irradiation at resonant frequencies, plasmonic nanomaterials strongly interact with photons, rapidly exciting electrons to an oscillating state and generating hot electrons within 1–100 femtoseconds. Afterward, these heated electrons cool down to a low-energy state via either radiative emission or electron-electron scattering. The latter process causes a rapid elevation in the localized surface temperature of plasmonic nanomaterials by redistributing energy among electrons of lower energy level, enhancing photon interactions and promoting heat transfer to the crystal lattice.[209] A traditional photothermal conversion process consists of three essential steps: 1) light harvesting, 2) light-to-heat conversion, and 3) heat transfer. First, the light-harvesting ability exhibited by photothermal materials indicates their capacity to absorb incident photon energy. The overall absorptance A(θ) of a light-absorbing material at a specified incidence angle of θ can be described as:[210,211]

$$A\ (\theta) = \frac{\int_{\lambda_{\min}}^{\lambda_{\max}} [1 - R\,(\theta,\ \lambda) - T\,(\theta,\ \lambda)]\, P\,(\theta, \lambda)\, d\lambda}{\int_{\lambda_{\min}}^{\lambda_{\max}} P\,(\lambda)\, d\lambda} \tag{11}$$

where $P(\lambda)$ stands for the radiation power of the incident light, and λ_{max} and λ_{min} denotes the maximum and minimum wavelengths of the incident light; and $R(\theta,\lambda)$ represents the light-absorbing materials' total reflectance at the wavelength λ, while $T(\theta,\lambda)$ represents the material's transmittance at the wavelength λ.[210] In the scenario where photothermal materials homogeneously dispersed within a semitransparent matrix, the absorptance of light follows Beer−Lambert's law:[210]

$$I\ = I_0\ e^{-kcl} \tag{12}$$

where I is the light radiation intensity after the absorption, and I_0 is the light radiation intensity before the absorption. κ, c, and l correspond to the extinction coefficient, particle concentration, and the length of the optical path, respectively.[210] Next, the light-to-heat conversion efficiency can directly quantify the absorbed

f) Immunofluorescence images illustrating the neurogenic differentiation of hMSCs on 4D-printed nanohybrid and the UV-cured counterparts. Panels a–f are reprinted with permission.[57] Copyright 1999–2023, John Wiley & Sons. g,h) 4D-printing of nanocellulose fibers reinforced SMP composites. g) Preparation of the PCL/PBAT/CNFs nanocomposite filaments used for FDM printing. h) The thermo-responsive climbing plant tendrils with spiral and self-deforming soft gripper of spiral structure. Panels g,h are reprinted with permission.[177] Copyright 2023, Elsevier B.V. i–k) Biomimetic 4D printing of nanocellulose. i) Schematic of programming localized anisotropy via biomimetic 4D printing, the alignment of nanocellulose within the ink can be controlled via the printing pathway. j) The shape-morphing behavior was manipulated by the printed patterns. k) By controlling the path of printing, the same printed structure exhibited different 4D performance. Panels i–k are reprinted with permission.[115] Copyright 2023, Springer Nature.

Table 5. Nanomaterials as photothermal fillers in 4D printing studies.

Nanomaterial	Nanomaterial Modification/Treatment	Material	Printing Technique	Stimuli	Key Features Incorporated Due to the Addition of Nanomaterials	References
AuNPs	Low Concentration	EA, IBOA, HDDA	DLP	LED (520–530 nm)	• Nanomaterial density: 0.05 phr in ink. • Responsiveness to LED irradiation. • Efficient photothermal effects: 25 → 80 °C change in 15 min light exposure (v/s negligible change in pure SMP).	[202]
AuNRs	AuNR–NIPAm/ AuNR-PEG	PNIPAm Gel	MPL	NIR	• Nanomaterial density: 0.38 particles per μm3 in ink. • Efficient photothermal effects induced by laser irradiation.	[203]
CuSNPs	PVP-stabilized CuSNPs	PU	Mold Casting	UV&Xe Light	• Nanomaterial concentration: 0.5 wt.%. • Responsiveness to Xe irradiation. • Time for full recovery: 63 s (v/s incomplete recovery in neat SMP).	[204]
GNPs	Physical Mixture	BDE/PBE/DA	Customized Multiple Printing Methods	NIR	• Nanomaterial concentration: 16 wt.%. • Efficient photothermal effects induced by laser irradiation. • Imparted higher material rigidity. • Improved electrical conductivity: 1.27 × 10–4 S m^{-1} (v/s non-conductive pure SMP).	[12]
	Physical Mixture	BDE/PBE/DA	Customized Multiple Printing Methods	NIR	• Nanomaterial concentration: 15 wt.%. • Higher Tensile moduli at 60 °C: ≈3 times (v/s neat SMP). • Slower thermoresponsive shape recovery time. • Efficient photothermal effects and shape recovery induced by NIR irradiation. • Improved electrical conductivity: 1.85 × 10–4 S m^{-1} (v/s non-conductive pure SMP).	[205]
rGOs	Sonication	LCE	DIW	NIR	• Nanomaterial concentration: 0.05 wt.%. • Efficient photothermal effects: RT → 70 °C change in 15 s NIR exposure (v/s 34 °C in pure SMP). • Reduced strength and stretchability (v/s pure SMP). • Slight reduction in T_g and storage modulus (v/s pure SMP).	[206]
CNTs	Dopamine-coated MWCNTs	PU/PCL/CNC	FDM	NIR	• Nanomaterial concentration: 3 wt.%. • Tensile strength improvement: 1.125 times (v/s neat SMP). • Elastic modulus improvement: ≈3 times (v/s neat SMP). • Improved thermal conductivity: ≈3 times (v/s neat SMP) • Efficient photothermal effects and shape recovery induced by NIR irradiation.	[207]
CB	Physical Mixture	PU	FDM	Sunlight	• Nanomaterial concentration: 10 wt.%. • Efficient photothermal effects: RT → 38 °C change in 300 s with 60 mW cm^{-2} Xe light exposure (v/s change to 27.5 °C in pure SMP). • Reduction in the T_g value: ≈30 °C (v/s ≈35 °C for neat SMP).	[197]

AA: Adipic acid; BDE: Bisphenol A diglycidyl ether; CNCs: Cellulose nanocrystals; DA: Decylamine; EA: Ethyl acrylate; HDDA: 1,6-Hexanediol diacrylate; IBOA: Isobornyl acrylate; NIPAm: N-isopropylacrylamide; PBE: Poly (propylene glycol) bis(2-aminopropyl) ether; PNIPAm: Poly(N-isopropylacrylamide); PVB: Poly(vinyl butyral); PVP: Polyvinylpyrrolidone; TBD: 1,5,7-Triazabicyclo (4.4.0) dec-5-ene; TMBPDGE: 3,3′,5,5′-Tetramethyl-4,4′-biphenyl diglycidyl ether; RT: Room temperature; Xe: Xenon.

energy transferred to thermal energy. The photothermal conversion efficiency η can be described as:[210,212,213]

$$\eta = \frac{Q}{E} = \frac{cm\Delta T}{pst} \quad (13)$$

where the terms – Q, E, c, m, ΔT, p, s, and t corresponds to the generated thermal energy, total light energy, specific heat of the photothermal material, mass of the photothermal material, change in temperature, light source's power density, radiation area, and radiation time, respectively.[210,212] Finally, the generated heat will be further transferred to other materials with lower temperature or dispersed to the surrounding environment. The conduction energy can be expressed as:[210,214]

$$Q_{\text{cond}} = \frac{ks}{L}\left(T - T_{obj}\right) \quad (14)$$

where k, s, L, T_{obj}, and T denote the thermal conductivity of the photothermal material, surface area available for heat transfer, length of the light absorber available for heat conduction, the steady temperature of the heat transfer object and the light absorber, respectively.[210,214] These mathematical equations mentioned above offer efficient ways to understand the mechanism of photothermal conversion, leading to the optimal use of photothermal responsive materials in 4D printing.

Noble metals (e.g., Au, Ag, etc.) nanomaterial and their hybrids have been widely investigated for the fabrication of photothermal-responsive material in 4D printing due to their excellent LSPR. However, metal nanomaterials have a tendency to agglomerate within the SMP nanocomposites at high concentrations, leading to uneven mechanical properties, inconsistent electrical conductivity, poor thermal conductivity, and even challenges during the manufacturing process. To address this issue, various strategies have been developed, such as NP surface modification or maintaining the NP solution at a low concentration to prevent agglomeration.[215] For example, thiol modification of metal NPs allows for the stabilization of noble metal NPs within a polymer matrix.[216,217]

AuNPs are nano-structured gold particles ranging from 1 to 100 nm, which are often spherical but can also be of other shapes, such as rods, triangles, and even urchins.[218] By varying their size and/or shape, AuNPs display plasmon resonance in the visible to NIR range, giving them unique optical characteristics.[219] Moreover, AuNPs also possess unique electronic and chemical properties that facilitates their application in biomedicine, such as drug delivery, imaging and bioelectronics.[220] Taking advantage of AuNPs' LSPR effect, Wang et al. fabricated acrylate-based nanocomposites with light-induced 4D shape change actuated by a light-emitting diode (LED) light with a wavelength of 520–530 nm.[202] Under LED light irradiation, the samples' temperature gradually increased, with the saturated temperature rising alongside the concentration of AuNPs in the samples. To actuate the 4D effect, the sample with 0.05 phr of AuNPs was selected, considering that 1) a higher concentration makes the sample fragile, 2) a lower concentration demonstrated significant enough photothermal effects, reaching 81 °C after 15 min of irradiation, and 3) maintaining a lower concentration prevented agglomeration and need for further modification to AuNPs. More importantly, the 4D shape-memory performance, particularly the response time, can be tuned by modifying the AuNPs concentration in the matrix, as it is positively correlated with the temperature's increasing rate and saturation temperature (**Figure 6**a,b). But, the inclusion of AuNPs had little impact on the R_f and R_r of the material, with both exceeding 95%.

Gold nanorods (AuNRs) are an elongated form of AuNPs. Compared to the perfect spherical symmetry of AuNPs, AuNRs possess an anisotropic structure, endowing them with two distinct LSPR modes: transverse and longitudinal modes.[221] As the length-to-ratio increase, the longitudinal dipole plasmon wavelength of AuNRs increases proportionally, extending from the visible to the IR region.[222] Taking advantage of the plasmonic heating properties of AuNR and the nanometer-scaled resolution of multiphoton lithography (MPL) printing, Nishiguchi et al. fabricated a soft 4D actuator with micrometer-scaled structure using thermoresponsive poly(N-isopropylacrylamide) (PNIPAm) and AuNRs.[203] As illustrated in Figure 6c, by controlling the printing density, a two layered structure, consisting of a static layer (high density) and dynamic layer (low density), was fabricated. When exposed to NIR stimulus, the difference in responsiveness between two layers results in internal stress, leading to ultrafast, reversible shape morphing, involving both twisting and falling motions (Figure 6d).

Copper sulfide nanoparticles (CuSNPs) as an effective NIR absorption agent, have also been researched in 4D printing as photothermal fillers. As a semiconductor, the NIR absorption in CuSNPs is different from that in gold nanostructures. The photothermal conversion of CuSNPs derives from energy band-band transition, while the absorption of gold nanostructure results only from LSPR.[223] Besides, in recent reports, strong NIR absorption performance induced by LSPR has also been observed in CuSNPs.[224] Unlike gold-mediated nanostructures, CuSNPs demonstrate enhanced resistance to the influence of the surrounding environment or solvent during in vivo delivery, thanks to their special photothermal effects.[225,226] Given their unique properties, CuSNPs are gradually emerging as promising agents in biomedicine, for instance, molecular imaging, drug delivery, and especially photothermal therapy.[227] In 4D printing, Vitola et al. incorporated polyvinylpyrrolidone (PVP)-stabilized CuSNPs into PU, synthesizing a biocompatible nanocomposite whose 4D SMEs were able to be actuated by Xe light.[204] Notably, it was observed that the addition of the NPs to the SMPs led to oversaturation effects, resulting in overheating of the material and impaired mechanical folding.

Alternatively, thermal vibration is another commonly observed mechanism in photo-responsive 4D constructs containing organic nanomaterials, exemplified by carbon-based nanomaterials.[228] Upon absorbing light of the appropriate wavelength, the loosely bound electrons in the organic nanomaterials are photo-excited from π to π^* orbitals. Subsequently, through electron-electron-phonon coupling, energy is transferred to the vibrational modes within the atomic lattices, resulting in a macroscopic increase in temperature, a process known as the π–π^* transition.[208]

As a representative carbon-based nanomaterial, GNPs demonstrate exceptional photothermal conversion properties with wide-ranging and wavelength-universal absorption spanning form visible to the NIR spectrum.[229] In particular, GNPs are able to absorb ≈48% of incident NIR light, reaching a significant

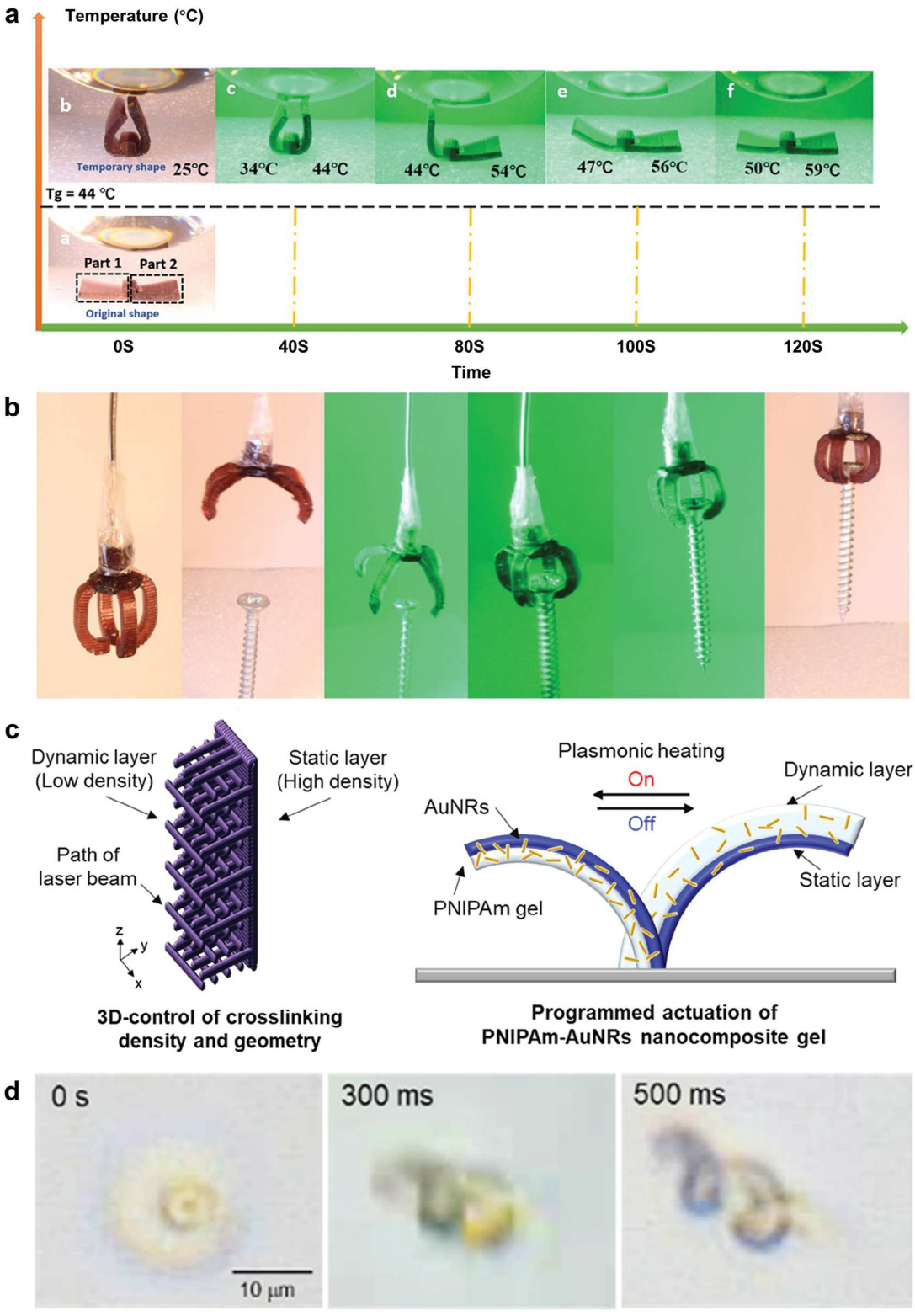

Figure 6. Metal-based nanomaterials as photothermal fillers. a,b) AuNPs-embedded 4D structure actuated by an LED light. a) Evaluation of shape-memory performance using DLP printed structures with a single T_g and two concentrations of AuNPs (left: 0.02 phr and right: 0.05 phr). b) A photo-actuated smart griper using AuNPs-embedded SMP. Panels a,b are reprinted with permission.[202] Copyright 1999–2023, John Wiley & Sons. c,d) AuNRs embedded hydrogel whose 4D effect is actuated by NIR light. c) Schematic and image of 4D printing of the AuNRs embedded hydrogel. d) Phase-contrast images of the two-layered 4D MLP-printed helix after laser exposure for 300 and 500 ms. Panels c,d are reprinted with permission.[203] Copyright 2022, American Chemical Society.

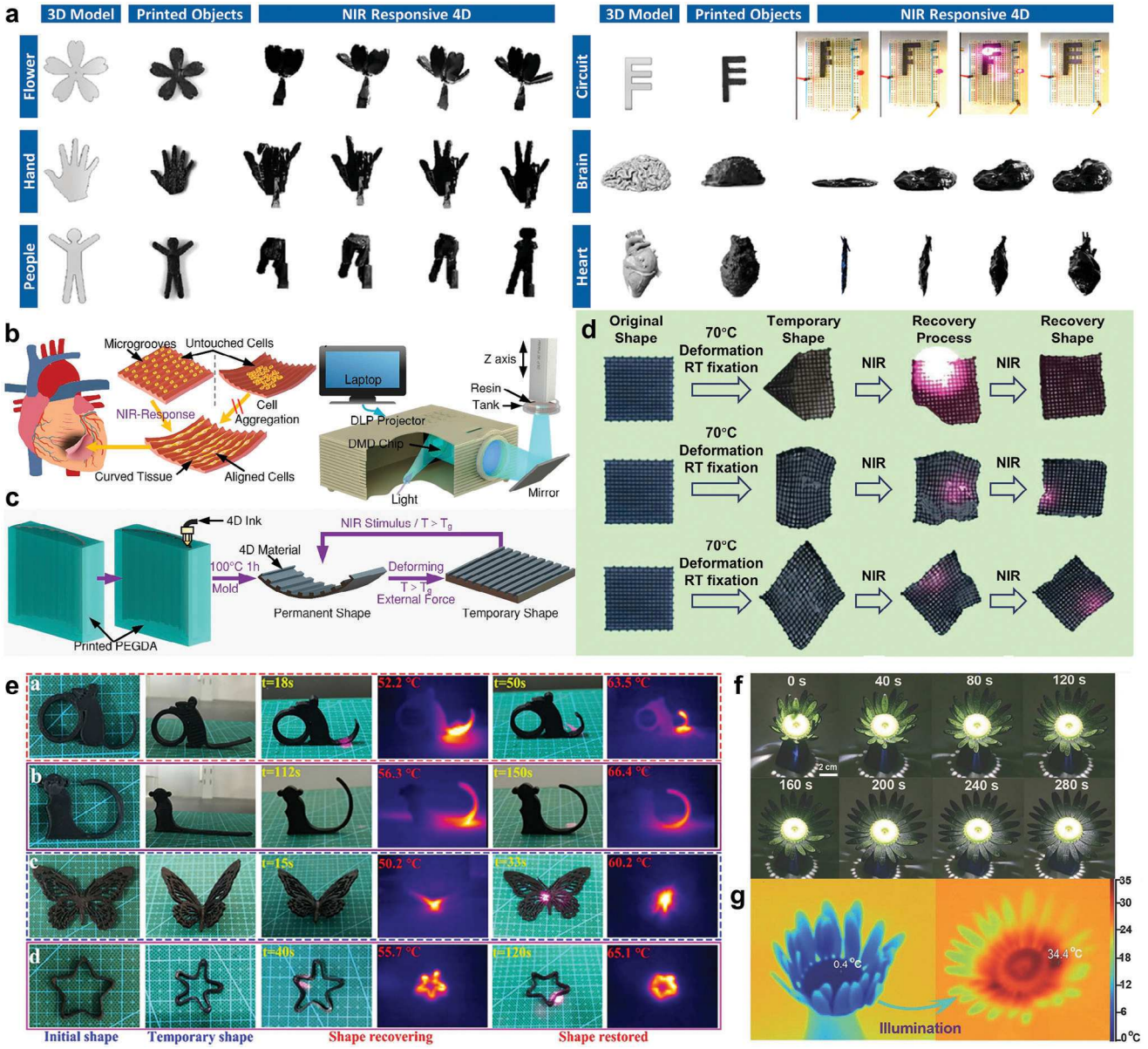

Figure 7. Carbon-based nanomaterials as photothermal fillers. a) NIR-responsive epoxy-based SMPs fabricated by doping GNPs, and using the nanocomposite, a series of NIR-responsive structures were fabricated. Panels a is reprinted with permission.[12] Copyright 2023, Springer Nature. b,c) Development of NIR-responsive cardiac patch using GNPs doped epoxy-based SMP. b) Schematic of a cell-laden cardiac patch with adjustable curvature, from a flat surface to a curved one and the setup of the DLP printing system for its fabrication. c) Schematic of the fabrication process of the 4D cardiac patch with a micro-aligned pattern. Panels b,c are reprinted with permission.[205] Copyright 2023, American Chemical Society. d) rGOs as NIR-responsive fillers. Partially actuated shape memory performance actuated by NIR illumination. Panel d is reprinted with permission.[206] Copyright 1999–2023, John Wiley & Sons. e) CNTs as NIR-responsive fillers. NIR induced SME of 4D printed structure a) mouse, b) monkey, c) butterfly, and d) star. Panel e is reprinted with permission.[207] Copyright 2023, Elsevier B.V. f,g) CB as photothermal filler in photothermal-responsive SMP. f) The 4D printed structure with a sunflower pattern change from a bud to bloom under light illumination. g) The infrared picture of the 4D printed sunflower structure before and after illumination. Panels f,g are reprinted with permission.[197] Copyright 1999–2023, John Wiley & Sons.

photothermal conversion efficiency of ≈65%.[230] Cui et al. doped GNPs into a smart epoxy-based SMP, resulting in a NIR-responsive nanocomposite with promising biomedical applications (**Figure** 7a).[12] In the nanocomposite, graphene can be homogeneously dispersed, primarily due to the π–π stacking between rigid aromatic epoxy and graphene. With the introduction of graphene, the physical properties of nanocomposites also change. For example, the elevation of graphene concentration leads to a simultaneous increase in viscosity, tensile modulus, and thermal conductivity. However, in comparison to the pure material, the nanocomposite showed a lower modulus, suggesting that the introduction of GNPs had a detrimental effect on the intrinsic structure of the pure material. Apart from that, doping GNPs imparts conductivity to the nanocomposite, but this

property is evident only when the GNP content exceeds 12 wt.%, making it adequate for engineering electroactive tissues like cardiac and neural. In another study, using the same GNPs-doped nanocomposites, Wang et al. created a cardiac patch with a highly aligned microstructure via DLP-based printing, the curvature of which could be controlled remotely by NIR light (Figure 7b,c).[205] Because it is intended for biomedical applications, the T_{trans} of nanocomposite was optimized to 45 °C, a temperature slightly higher than human body temperature. Upon the illumination of NIR, the 4D printed construct underwent a spatiotemporal transformation that is actuated remotely. This process allowed for the uniform and spatial redistribution of tricultured cells, which also broadens the potential applications of 4D printing in the field of tissue engineering. As derivatives of GNPs, rGO also exhibit a significant photothermal effect due to their structural similarity to GNPs.[231,232] By doping rGO into LCE-based polymer networks (PNs), Gong et al. fabricated a NIR-responsive SMP (G/PNs) with reversible shape memory performance.[206] Using thiols as cross-linker, the G/PNs are able to be printed via UV-assisted DIW printing technique. As shown in Figure 7d, the 4D printed structure exhibited remotely and regionally controllable 4D shape morphing properties, exhibiting the potential in actuator and artificial muscles application.

CNTs are tubular structures composed of single or multiple-layer carbon atoms that are rolled up into a cylindrical shape.[233] According to the layer count, CNTs can be classified into two types: single-walled carbon nanotubes (SWCNTs), with a diameter of less than 1 nm, and multi-walled carbon nanotubes (MWCNTs), consisting of multiple interlinked nanotubes arranged concentrically, with diameters ranging from a few to over 100 nm.[234] CNTs and GNPs share a common structural element: a periodic array of annelated benzene rings. Despite difference in dimensions and curvature, they are sufficiently comparable to exhibit a photothermal effect, which efficiently convert NIR light into heat. Bi et al. developed a FDM-printable shape memory nanocomposite with NIR-responsiveness by incorporating dopamine (DA)-coated MWCNTs (PMWCNTs) into the SMP matrix.[207] In the nanocomposite, MWCNTs served as the photothermal filler, and DA was employed to modify MWCNTs with non-covalent functional groups, enhancing the interface interaction between the filer and the matrix. Due to the abundance of -OH and -NH- groups on DA coating, hydrogen bonds can easily form between PMWCNTs and the polymer matrix, facilitating homogeneous dispersion within the matrix. Moreover, hydrogen bonds also enhance the mechanical properties of the nanocomposite. With 3 wt.% PMWCNTs, the nanocomposite achieved a maximum tensile strength of 46.1 MPa and an elongation at break of 1185.6%. However, an excess of PMWCNTs (5 wt.%) formed a separation structure, leading to reduced tensile strength and elongation at break. Compared to the pure composite, the nanocomposite with 3 wt.% PMWCNTs demonstrated similar shape memory performance, with R_f and R_r both exceeding 90% and 75%, respectively. Furthermore, the nanocomposite can be processed into thermoplastic filaments and utilized in FDM printing. As illustrated in Figure 7e, a variety of NIR-responsive constructs were successfully printed.

Carbon black (CB), a finely divided form of carbon, is widely used to enhance the mechanical, electrical, and other physical properties of the medium in which it is dispersed.[235] Unlike GNPs, CB is composed of amorphous carbon particles with a disordered arrangement of carbon atoms. Additionally, CB can serve as a more cost-effective and readily available photothermal agent under visible light irradiation.[236] Yang et al. incorporated CB into PU to create a photo-responsive nanocomposite that can be printed using FDM.[197] Acting as a photothermal filler, the nanocomposite's maximum temperature increased with the rising concentration of CB in the polymer matrix, reaching the saturation temperature at 16 wt.% of CB, ≈40 °C (under a light intensity of 60 mW cm^{-2}). Meanwhile, the nanocomposite's T_g gradually decreased with the increasing CB content. As illustrated in Figure 7f,g, a sunflower-structured construct capable of blooming under sunlight was printed using FDM printing with the nanocomposite containing 10 wt.% CB and a T_g of 30 °C. Compared to photopolymerization printing techniques, FDM offers the advantage of not necessitating UV exposure, thereby circumventing the significant influence of UV illumination during the printing procedure, especially for UV-responsive material. This straightforward printing approach opens up opportunities for the design and manufacture of biomimetic smart devices and soft robotics.

3.3.2. Nanomaterials as Electrothermal Fillers

Electroactive printable materials represent a promising direction in the emerging field of 4D printing, driven by the increasing demand for faster, cost-effective methods to create electroactive devices through the development of printable inks for film-based application.[237] 4D printing of electroactive materials has demonstrated great potential for applications in areas such as memory storage, flexible electronics for wearable devices, and artificial muscles for robots.[238–241] SMPs are naturally electrically non-conductive. By incorporating conductive nanomaterials, such as carbon-based nanomaterials (e.g., GNPs and carbon nanofibers) and metal-based nanomaterials (e.g., AgNPs, AgNWs, etc.), SMP nanocomposite can be actuated using Joule heating – internal heating through electric current – getting rid of the need for direct heating for 4D effect activation (**Table 6**). Compared to structures directly actuated by heat, applying a voltage to electrodes at specific positions on the construct enables partial and precise actuation of the structure. Generally, the 4D actuation at different voltages depended on the electrothermal effect and the heat dissipation to the surroundings. Here, the voltage-dependent temperature change can be modeled using the theoretical equation:[242]

$$Q = \frac{V^2}{R} \tag{15}$$

where Q represents the amount of heat, V denotes the input voltage, and R stands for the resistance. If the heat dissipation is excluded, the temperature change can be simply described as:

$$\Delta T = \frac{Q}{cm} \tag{16}$$

where ΔT represents temperature change after applied voltage, c is the specific heat capacity of materials, and m is the weight of materials. When conductive nanomaterials are incorporated into polymers, the conductivity of nanomaterials, the heat transition

Table 6. Nanomaterials as electrothermal fillers in 4D printing studies.

Nanomaterial	Nanomaterial Modification/ Treatment	Material	Printing Technique	Stimuli	Key Features Incorporated Due to the Addition of Nanomaterials	References
MWCNTs	Sonication	PEGDA, HEMA	DLP	Voltage	• Nanomaterial concentration: 0.5 wt.%. • Imparted better shear thinning properties (v/s pure SMP) • Improved electrical conductivity: 5.8×10^{-1} S cm^{-1} (v/s non-conductive pure SMP). • Reduction in T_g value: 62 °C (v/s 70 °C in pure SMP) • Efficient electrothermal effects: ≈78 °C upon exposure to 175 V (v/s no change in pure SMP).	[110]
Carbon Nanofibers	Sonication	ESBO, BFDGE	DIW	Voltage	• Nanomaterial density: 5.6 vol%. • Improved electrical conductivity: $\approx 4.0 \times 10^{-1}$ S cm^{-1} (v/s non-conductive pure SMP). • Increase in the storage and rubbery modulus at 25 and 150 °C, respectively (v/s pure SMP). • Efficient electrothermal effects: shape recovery in 180 s upon exposure to 20 V, 150 mA source (v/s no change in pure SMP).	[243]
Silver-coated Carbon Nanofibers	Physical Mixture	PLA, DCM	DIW	Voltage	• Nanomaterial density: 10.6 vol%. • Improved electrical conductivity: ≈104 S m^{-1} (v/s non-conductive pure SMP). • Elastic modulus improvement: ≈1.3 times (v/s neat SMP). • Decrease in elongation at break: ≈4 times (v/s neat SMP). • Efficient electrothermal effects: ≈80 °C upon exposure to 1 V power source.	[244]
AgNPs	NA	LCE (RM257, EDDET, PETMP), Tango Black	Inkjet and DIW	Voltage	• Nanomaterial density: 49–53% (commercial conductive ink used to create conduction framework). • Efficient electrothermal effects observed, resulting in 4D shape change.	[71]
AgNWs	NA	PLA, CSP	FDM	Voltage	• Nanomaterial density: NA (nanomaterials deposited over 3D printed structures). • Efficient electrothermal effects: RT → 55 °C upon exposure to 2.8 V power source in 50 s.	[112]
GNPs	Physical Mixture	GPLA	FDM	Voltage	• Nanomaterial concentration: Commercial GPLA • Efficient electrothermal effects	[98]
SWCNTs	Chemical Modification (Acid Treatment) and Physical Mixture	PU	FDM	Voltage	• Nanomaterial concentration: NA. • Slower recovery rate at lower temperature (v/s pure SMP using direct heating). • Efficient electrothermal effects (v/s pure SMP).	[245]

BFDGE: Bisphenol F diglycidyl ether; CNTs: Carbon nanotubes; CSP: Conductive silver paste; DCM: Dichloromethane; DIW: Direct-ink writing; DLP: Digital light modeling; EDDET: 2,2′-(ethylenedioxy) diethanethiol; ESBO: Epoxidized soybean oil; GPLA: Graphene-PLA; HEMA: 2-hydroxyethyl methacrylate; PCO: Polycyclooctene; PE: Polyethylene; PETMP: Pentaerythritol tetrakis (3-mercaptopropionate); PLA: Polylactic acid; RM257: 1,4-bis- [4-(3-acryloyloxypropyloxy) benzoyloxy]−2-methylbenzene; RT: Room temperature; NA: not available.

efficiency, and the resistance of the polymer matrix will also be considered. The equation can be modified based on the different composite systems.

Generally, carbon-based materials exhibit electrical conductivity due to the presence of delocalized electrons, which can move freely within the material. The specific arrangements of carbon atoms and the overlap of electron orbitals facilitate the movement of these delocalized electrons, enabling the materials to conduct electricity. As a zero-overlap semimetal, GNPs are composed of sp^2-bonded carbon atoms that share three valence electrons with their neighboring carbon atoms on the 2D plane, leaving one highly-mobile electron (π electrons) in the

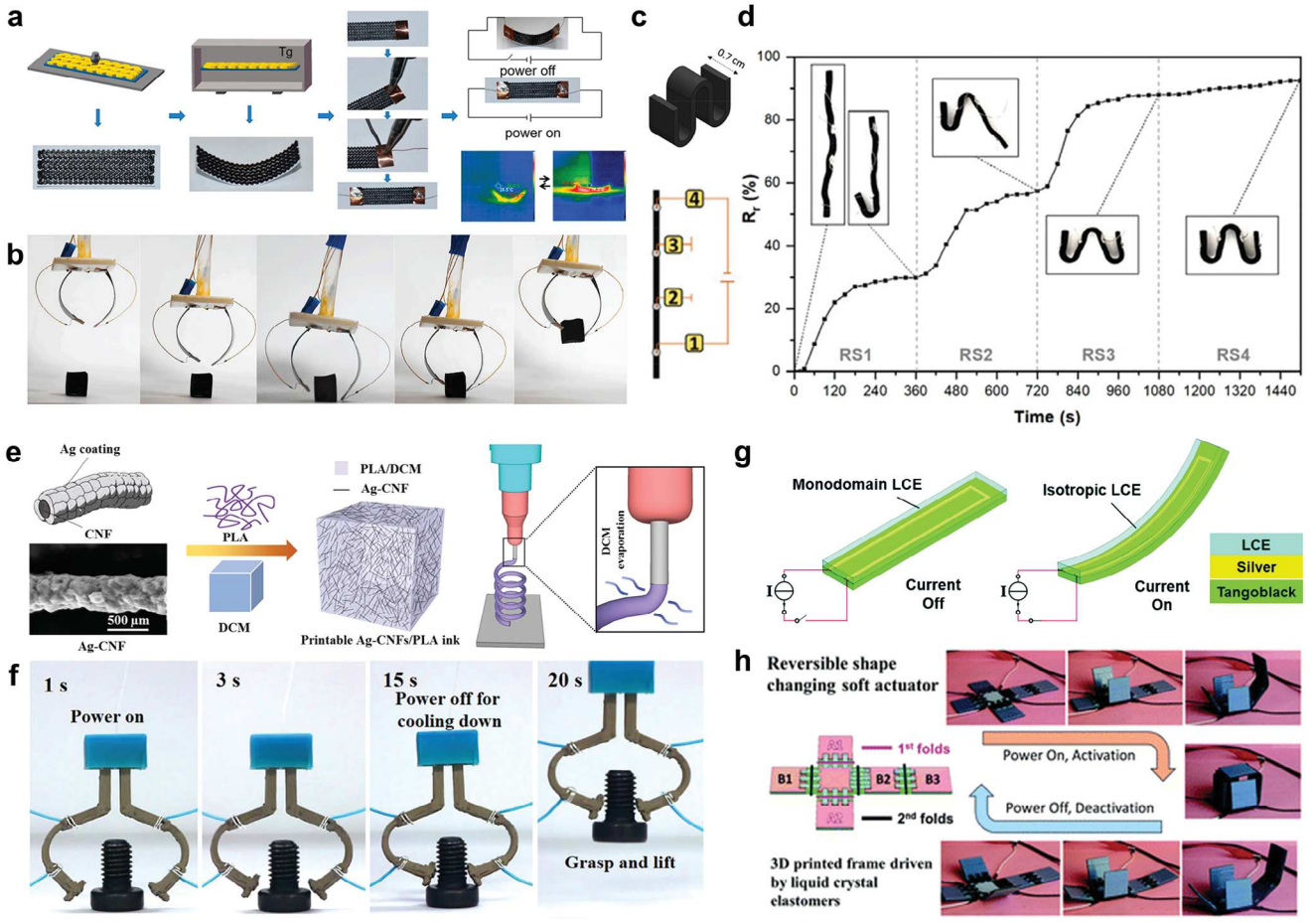

Figure 8. Nanomaterials as electrothermal fillers. a,b) 4D printing of reversible actuator using GPLA. a) Fabrication process of an electro-actuated reversible actuator. b) Intelligent mechanical claw, fabricated using the 4D printed actuator, is capable of detecting the shape of objects according to the feedback resistance signal. Panels a,b are reprinted with permission.[98] Copyright 2023, Elsevier B.V. c,d) 4D printing of the SMP nanocomposites doped with CNTs, featuring remote, modular, and selective controllability. c) Schematic of CAD model of the zig-zag structure with four electrodes designed for selective and modular shape recovery. d) Stepwise shape memory performance by selectively actuating the electrodes. Panels c,d are reprinted with permission.[110] Copyright 1999–2023, John Wiley & Sons. e,f) 4D printing of Ag@CNF/PLA nanocomposite. e) Illustration of the structure of silver-coated carbon nanofiber, Ag@CNF/PLA, and solvent-casting printing (SC printing) of Ag@CNF/PLA nanocomposite. f) Illustration of the 4D printed electric-actuated smart gripper using Ag@CNF/PLA. Panel e–f are reprinted with permission.[244] Copyright 2023, American Chemical Society. g,h) Reversible smart actuators fabricated using AgNPs incorporated LCE. g) Schematic of the structure and activated/deactivated state of the reversible soft actuator. h) Schematic and snapshots of the folding box using the smart actuator as hinges. Panels g,h are reprinted with permission.[71] Copyright 2023, Royal Society of Chemistry.

third dimension, which is the reason why GNPs break so many records not only in terms of electricity conduction, but also in terms of strength and heat conduction.[246,247] Given the properties of GNPs, they have been extensively explored as conductive/electrothermal fillers in 4D printing of electroactive materials, with notable success, such as the commercialization of graphene-PLA (GPLA), a well-established conductive 3D printing filament.[185,248] Using commercial GPLA, Wang et al. developed a strategy for fabricating a reversible actuator with inherent strain self-sensing capabilities through the structural design of a bilayer composite by FDM printing (**Figure** 8a).[98] The bilayer structure comprises a GPLA layer as the active thermoplastic layer and a paper substrate as the passive limiting layer. Reversible deformation is achieved through FDM printing, where prestrain stored in the GPLA structure causes controlled shrinkage at the T_g. The paper substrate restrains the shrinkage, converting it into programmed bending. Subsequent heating and cooling cycles enable reversible shape changes. The self-sensing function is achieved by measuring the resistance, which changes as the contact surface between the printed GPLA and paper is altered during deformation. Using this strategy, an intelligent mechanical claw capable of perceiving the shape of objects was developed, as illustrated in Figure 8b.

As mentioned earlier, CNTs share some properties similar to GNPs, with excellent electrical conductivity being one of them.[246] In regard to this property, Nguyen et al. developed a FDM printable nanocomposite comprising SWCNTs and PU.[245] To attain homogeneous dispersion of SWCNTs within the PU matrix, chemical modification was performed using acid treatment, creating m-SWCNTs. The modification

introduced additional carboxyl (-COOH) functional groups to the ends and sidewalls of the m-SWCNTs, facilitating the interaction through the formation of hydrogen bonds. The 4D printed sample exhibited electro-responsiveness. Applying an electric current (35 V, 0.024A) to the sample's electrodes heated it beyond its T_g (25 °C), and the structure recovered to its original shape in 48 s. In another research, Cortés et al. prepared an electro-activated SMP nanocomposite for DLP printing, consisting of PEGDA/poly(hydroxyethyl methacrylate (PHEMA) matrix embedding MWCNTs.[110] The addition of a small amount of MWCNTs (0.5 wt.%) can render the matrix electrically conductive, albeit requiring higher voltages for efficient electrothermal effects (78 °C under 175 V exposure). Interestingly, as shown in Figure 8c,d, by selectively activating the electrodes, a modular and selective electro-actuated shape recovery was achieved, demonstrating the huge potential in 4D smart devices and soft robots.

Unlike concentric CNTs, which have a completely hollow core, carbon nanofibers exhibit stacked truncated conical or planar layers running along the length of the fiber.[249] By doping carbon nanofibers into epoxy-based SMP matrix, Rodriguez et al. fabricated a electroactive ink that can be printed via DIW printing.[243] In the system, carbon nanofibers serve dual functions as a rheological modifier and electrothermal filler. With an increase in carbon nanofiber concentration, the ink's viscosity gradually rises, displaying shear-thinning behavior. Inks loaded with over 4 vol% CNFs exhibit the required shape retention for constructing 3D objects. Further increasing the CNFs load to 5.6 vol%, the ink demonstrates both DIW printability and sufficient conductivity for achieving shape memory actuation through Joule heating. Apart from using pure carbon nanofiber as a filler, modified nanofibers with enhanced properties are frequently investigated as well. Wei et al. employed an electroless depositing method to coat silver on CNFs, resulting in a hybrid silver-coated nanomaterial, Ag@CNF, which exhibited higher conductivity than pure counterparts.[244] In their research, dichloromethane (DCM) was used as a solvent to dissolve PLA and disperse Ag@CNF homogeneously. Taking advantage of its high volatility of the solvent, a new DIW-based printing method, namely solvent-casting printing (SC printing), was developed (Figure 8e). Using the nanocomposite inks, an electric-actuated smart gripper was fabricated (Figure 8f), showcasing its potential in flexible electronics, smart actuator designs, and robotics.

Metals conduct electricity by allowing free electron movement between metallic atoms, as these electrons are not bound to specific atoms or covalent bonds. In addition to electrical conductivity, metallic nanomaterials demonstrate additional or enhanced properties due to nanoscale effects. For instance, AgNPs exhibit size-dependent optical properties due to LSPR and their absorption of light at specific wavelength, determined by the size and shape of the NPs.[250] Spherical AgNPs with an approximate diameter of 2.6 nm (λ_{max} = 393 nm) appear light yellow; a mixture consisting of 91.2% of spherical NPs (d = 9.5 nm) and 7.9% of AgNRs (size: 13.5 nm × 10.5 nm, λ_{max} = 461 nm) exhibits an orange-red color.[251] The utilization of conductive nanomaterials as ink for producing electronic circuits and devices, particularly on flexible substrates, has been a subject of research for many years and has evolved into a well-developed discipline known as printed electronics.[252] Against this background, some printable metallic NPs ink with conductivity have been developed and commercialized, such as ME 603 – a AgNPs based printable conductive ink developed by DuPont Company. Using this commercial AgNP ink (DuPont ME603), Yuan et al. engineered an electrically-actuated smart hinge featuring a three-layer structure comprising commercial resin Tango Black, AgNPs ink, and LCE through a combination of DIW and inkjet printing techniques (Figure 8g).[71] The smart hinges were further used to create a smart box whose folding process could be precisely controlled (Figure 8h). AgNWs are nanoscale wire-like structures of silver nanomaterials with an aspect ratio greater than 10.[253] Using them, Shao et al. created a 4D printed construct featuring a sandwich structure: PLA-printed base with microgroove, AgNWs network and conductive silver paste (CSP).[112] The printed structure of PLA/AgNWs exhibited a swift response under the applied voltage, taking only 4 seconds to recover from its temporary shape to its permanent shape. Utilizing this structure, a smart gripper was fabricated. When energized, the gripper is able to grasped a ball in an icy temperature environment, indicating that its actuation is not affected by ambient temperature.

3.3.3. Nanomaterials as Magnetothermal Fillers

In order to fabricate 4D printed structures with multifunctionalities, magnetic nanoparticles (MNPs) have also attracted much attention. MNPs are nanostructured magnetic metals, such as iron and their oxide forms (e.g., Fe_3O_4, and Fe_2O_3), exhibiting paramagnetic, ferromagnetic, or superparamagnetic characteristics.[254] Magnetocaloric effect (MCE) is the heating or cooling of a magnetic material when the applied MF changes. Magnetic heating is usually applied for the 4D printing of SMPs. When subjected to an alternating MF, the MNPs incorporated SMPs experience hysteresis loss and eddy current loss, resulting in the generation of inductive heat that raises the temperature above T_{trans} to actuate SME.[255] A high heating efficiency or inductive specific absorption rate (SAR) is required for MNPs.[256] Apart from the applied ac MF amplitude and frequency, SAR depends on the saturation magnetization, particle size, concentration, composition, and effective anisotropy of MNPs.[256] The heat production is mainly attributed to the energy loss by overcoming the rotational energy barrier.[257] Generally, the relaxation effect is dominated in heat production; therefore, the magnetic heating performance of MNPs mainly originates from Brownian relaxation and Néel relaxation.[256,257] The Brown relaxation refers to the physical rotation of MNPs, while the Néel relaxation refers to the rotation of individual magnetic moments within MNPs.[257] When MNPs are incorporated in the polymer matrix, the Brownian relaxation can be negligible; therefore, the main heating mechanism is Néel relaxation-induced hysteresis loss. The Néel relaxation can be expressed as:[256]

$$\tau_N = \tau_0 \exp\left(\frac{KV}{kT}\right) \quad (17)$$

where τ_N is the Néel relaxation time, τ_0 is the time constant ($\approx 10^{-9}$ s), k is the Boltzmann's constant, K is the anisotropy constant, and V is the volume of NP.[256] As such, magnetic heating is majorly determined by the magnetic anisotropy coefficient K and volume of NP V. For the nanocomposites, the size, shape, concentration, and space distribution of MMPs will largely affect

Table 7. Nanomaterials as magnetocaloric fillers in 4D printing studies.

Nanomaterial	Nanomaterial Modification/Treatment	Material	Printing Technique	Stimuli	Key Features Incorporated Due to the Addition of Nanomaterials	References
Fe_3O_4 NPs	Physical Mixture	PLA	DIW	30 kHz MF	• Nanomaterial concentration: 25 wt.%. • Imparted better shear thinning properties (v/s pure SMP) • Elastic modulus improvement: ≈1.12 times (v/s pure SMP). • Decrease in elongation at break: ≈1.875 time (v/s pure SMP) • Shift in T_g value: 53.13 °C (v/s 47.88 °C in pure SMP). • Efficient magnetothermal effects: shape recovery within 23 s of MF exposure.	[97]
	Physical Mixture	PLA	DIW	30 kHz MF	• Nanomaterial concentration: 10 wt.%. • Higher Elastic modulus (v/s pure SMP). • Efficient magnetothermal effects: shape recovery within 22 s of MF exposure.	[69]
	Sonication	AESO/IBOMA	DLP	30 kHz MF	• Nanomaterial concentration: 5 wt.%. • Reduction in Elastic modulus: ≈2 times (v/s pure SMP). • Decrease in elongation at break: ≈3 time (v/s pure SMP) • Shift in T_g value: 53.13 °C (v/s 47.88 °C in pure SMP). • Efficient magnetothermal effects: 82% shape recovery within 40 s of MF exposure.	[264]

AESO: Acrylate epoxy soybean oil; BA: Butyl acrylate; IBOMA: Isobornyl methacrylate; LDPE: Low-density polyethylene; Org-MMT: Organically modified montmorillonite; TFX: Polyetherurethane.

the MCE, which further influence the 4D actuation performance of SMPs.

Among MNPs, Fe_3O_4 NPs offer significant promise in biomedical applications because of their excellent biocompatibility, magnetic properties, and electronic conductivity.[258] Besides, Fe_3O_4 has been approved by the FDA as an ingredient for iron deficiency therapy and as a contrast agent in magnetic resonance imaging.[259–261] In regard to this, Fe_3O_4 has been widely investigated in 4D printing as shown in **Table 7**. As aforementioned, metal NPs tend to aggregate and form clusters within a suspension. To achieve homogeneously dispersed Fe_3O_4 SMP nanocomposites, physical methods such as continuous stirring and ultrasonication have been widely employed.[262,263] While continuously stirring Fe_3O_4 NPs in DCM with dissolved PLA and benzophenone (BP) for 24 h, Wei et al. successfully created a 4D nanocomposite with uniformly dispersed Fe_3O_4 (**Figure 9a**).[97] Using the nanocomposite, the research team fabricated a self-expandable helical scaffold that can be remotely actuated by MF through DIW printing and in situ UV cross-linking (Figure 9b). As shown in Figure 9c, when exposed to a 30 kHz MF, the helical construct expands in 10 s, demonstrating significant potential for applications in vascular stents. In another study from the same lab, Lin et al. fabricated a remotely controllable occlusion device for congenital heart disease treatment (Figure 9c) using the method and same nanocomposite (but with lower Fe_3O_4 concentration (10 wt.%)).[69] In addition to being deployed under MF stimuli *in vitro* (Figure 9d–f), the 4D printed scaffold exhibited great biodegradability in the in vivo experiment. Using ultrasonic vibration, Huang et al. achieved homogeneous incorporation of Fe_3O_4 NPs into a photo-cross-linkable polymer matrix, resulting in a resin suitable for DLP printing.[264] The addition of NPs led to the formation of defects such as microvoid and cracks within the structure, significantly reducing the tensile strength and break elongation of the nanocomposite. Adding a moderate amount of NPs (1 and 3 wt.%) increased the elastic modulus by 17.1% and 11%, respectively, attributed to the rigidity of the particles compared to the resin matrix and their uniform dispersion in the resin at lower concentrations. Additionally, structures with Fe_3O_4 NPs exhibited a higher shape fixity ratio but lower shape recovery ratio. Those with higher NP concentration showed a faster recovery speed, attributed to the enhanced thermal conductivity resulting from the introduction of NPs.

3.3.4. Nanomaterials for Other Functionalities

The utilization of nanomaterials in 4D printing technology extends beyond serving as rheological modifiers and enhancers of 4D effects; it also introduces new stimuli-responsiveness. Researchers have also been exploring the potential of existing nanomaterials and creating customized nanomaterials with new functions for diverse purposes.

In different scenarios of 4D printing, the same nanomaterial might play different roles due to its different properties. For instance, as mentioned above, Fe_3O_4 NPs are capable of serving as a magnetocaloric agent to generate heat in 4D printing, which tends to overlook the force generated by magnetic attraction among magnets. Using Fe_3O_4 NPs and platinum nanoparticles

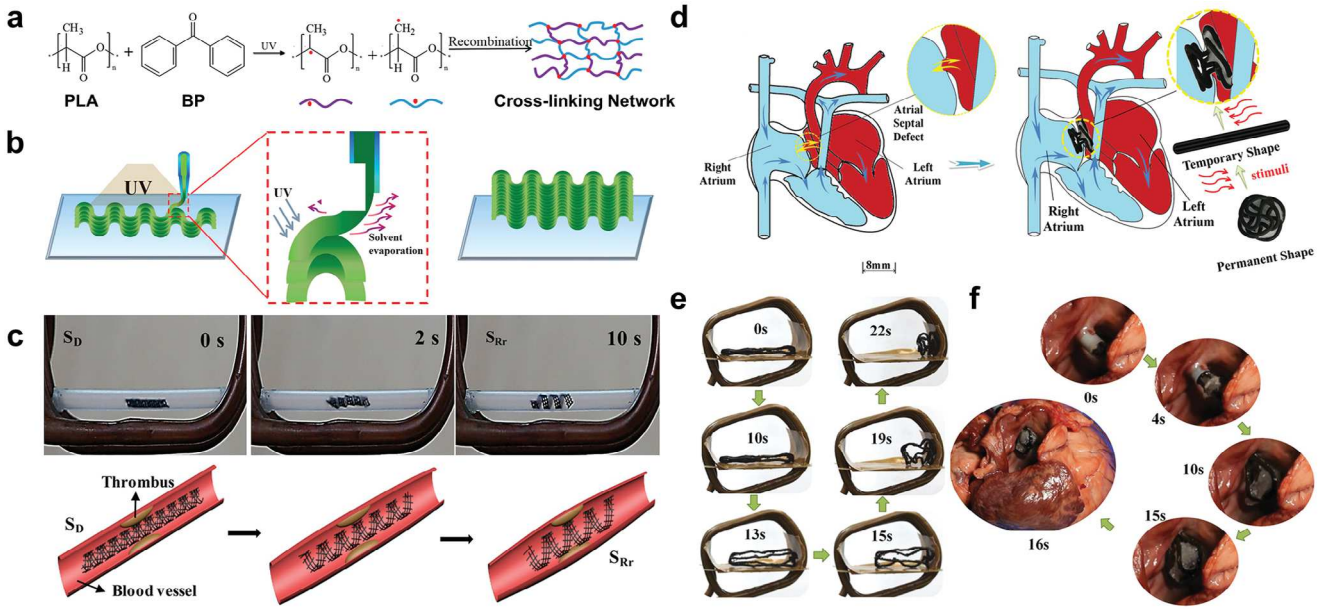

Figure 9. MNPs as magnetocaloric fillers. a–c) 4D printed magneto-responsive intravascular stents using Fe_3O_4 incorporated PLA. a) Schematic of printing mechanism and b) ink composition to form 4D active structures. c) Shape recovery of the printed stents under restrictive conditions triggered by alternating MF, suggesting its utility as intravascular stents. SD: shape deformed; SRr: shape recovered. Panels a–c are reprinted with permission.[97] Copyright 2023, American Chemical Society. d–f) 4D occluders activated by magnetics, created using PLA incorporated with Fe_3O_{44}. c) Schematic of the implantation of the 4D printed occluders. e) Controlled shape recovery behavior of the MF-actuated Fe_3O_4 doped PLA occluder. f) Feasibility test in porcine heart models *in vitro*. Panels d–f are reprinted with permission.[69] Copyright 1999–2023, John Wiley & Sons.

(PtNPs), Xin et al. developed 4D-printed shape-morphing micromachines that are capable of being navigated to travel in micronetworks.[265] Using direct DLW printing (femtosecond laser), a fish shape structure in micro-scale was printed, which consists of three main parts: 1) pH-responsive hydrogel, as the main body of the structure that is capable of undergoing shape-morphing under the stimulus of pH; 2) Pt NPs, as the catalyzer in hydrogen peroxide solution to generate bubbles, which provides the structure initial movement; 3) Fe_3O_4 NPs, the magnetic force generated from the interaction between Fe_3O_4 NPs and outside magnet is used for navigation. As illustrated in **Figure 10**a–i, by manipulating the hybrid bubble-magnetic actuated shape-morphing microfish (SMMF), it is able to pass through the complicated maze by fin morphing. Using the same materials but without Pt NPs, Xin et al. further developed the system and fabricated a shape-morphing microcrab (SMMC) that acts as a micro-gripper and an SMMF that is used for drug delivery. By adjusting the pH of the environment, the SMMC's claws can be controlled. Then, under the direction of an external MF, the SMMC migrates, allowing for the completion of cargo transportation (Figure 10j). The SMMF used for drug delivery can be manipulated to encapsulate and release drug (doxorubicin (DOX)) by adjusting pH (Figure 10k). In the *in vitro* study, the SMMF was successfully navigated to the designated location and release the drug, successfully killing the cancer cells (Figure 10l).

In addition to acting as an effective rheology modifier, silica NPs have been approved as "catalysts" in photopolymerization-based 4D printing, enhancing resin curability as reported by Choong et al. (Figure 10m).[145] nanosilica particles efficiently diminish light scattering within the polymer matrix by establishing heterogeneous nucleation sites, thereby significantly shortening the curing time. In DLP printing, the addition of 2.5 wt.% silica NPs into the resin significantly reduced the curing time for each layer from 4 to 0.7 s. Besides, the printed nanocomposites exhibited a ten-fold improvement in mechanical properties and a greater elongation of 85.2% compared to the pure SMPs. The introduction of silica NPs did not significantly impact the 4D performance of the nanocomposite, as evidenced by a shape recovery ratio within a high range of 87–90%.

However, sometimes, the existing nanomaterial cannot meet the needs of investigations. Thus, customized, or homemade nanomaterials with special functions are engineered. For instance, Fang et al. fabricated a nanostructure (named NCs) that was used to realize the controllable release of nerve growth factors (NGFs) in 4D NGCs.[266] The sandwich NCs consist of three layers: 1) rGO nanosheets, 2) a silica shell, and 3) a mesoporous carbon layer (Figure 10n,o). The NCs exhibited a strong interaction with NGFs, the release of which could be triggered by high-frequency MF. This allowed for achieving the on-demand release of NGFs, leading to the simultaneous stimulation of neural cells to improve their growth and differentiation. The conductive nature of the conduits also provided necessary electrical stimulation that had an additive effect on nerve regeneration. In the in vivo trial, rats with 10 mm sciatic nerve gaps were effectively repaired, and the therapeutic efficacy was equivalent to that of autografts.

Incorporating a temporal element and linked stimuli in 4D food printing allows for the production of printed food capable of undergoing controlled alterations in color, texture, and flavor triggered by internal or external factors.[267,268] This advancement offers a wide array of choices to consumers with a diverse range of options and caters to the specific needs of special groups. In order to stabilize curcumin, a 4D color stimulus-response

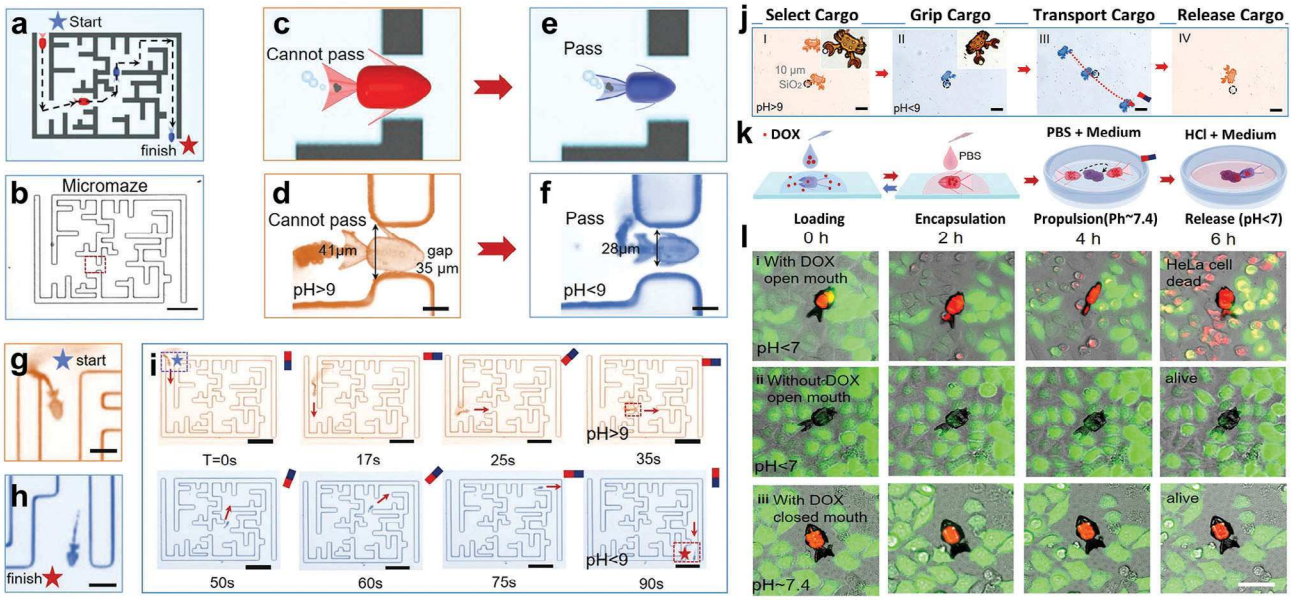

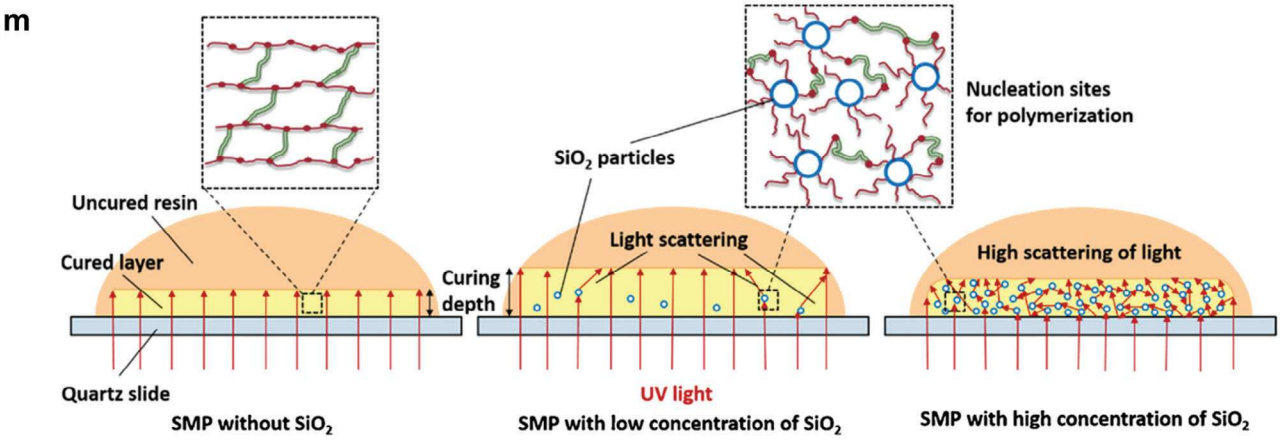

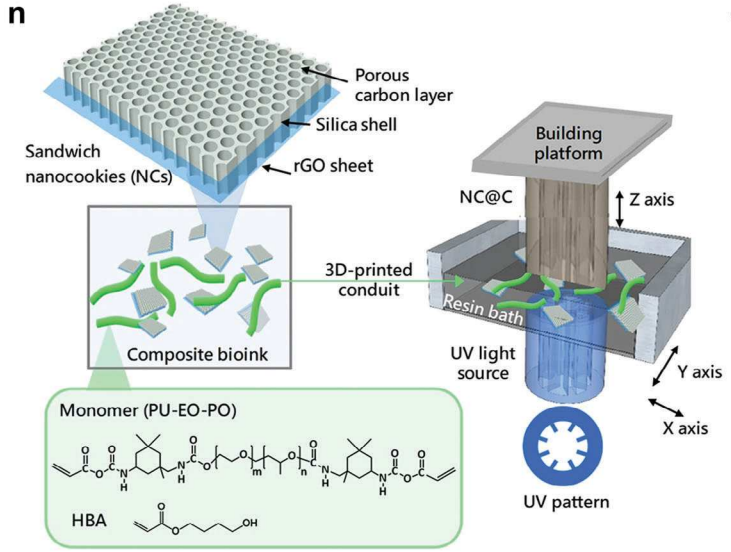

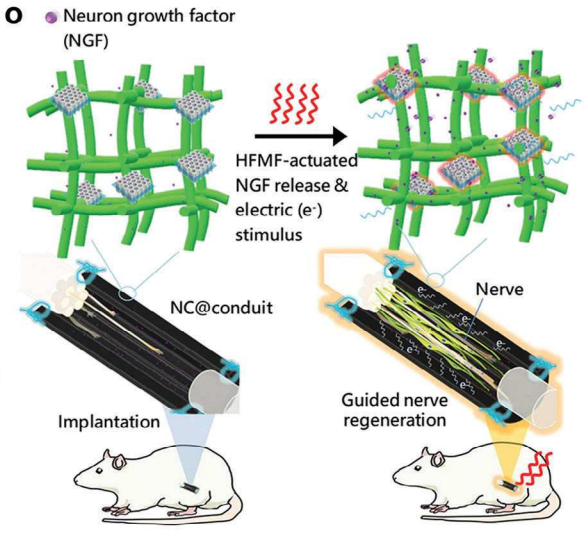

material that is usually in 4D food printing, Shen et al. fabricated a NP (G-WPI-NPs) by encapsulating curcumin (G) into whey protein isolate (WPI).[269] The G-WPI-NPs improved water-holding capacity and the rheological properties of printing inks based on a potato/xanthan gum mixture. Furthermore, the 4D-printed food samples' color shifted from a bright yellow to a dark yellow following various drying technique, demonstrating its potential as an indicator of dryness in the food industry.

4. Conclusion and Perspectives

In this review, we summarized and discussed the utilization of nanomaterials in 4D printing over the past years. Nanomaterials, characterized by their distinctive physical and chemical properties on the nanoscale, expand the horizons of material design and functionality. When integrated with the dynamic capabilities of 4D printing, a synergistic relationship emerges, amplifying their impact in various domains. Extensive studies have consistently demonstrated the efficacy of incorporating nanomaterials as a promising strategy to make improvements in 4D printing. In a nutshell, the incorporating NPs within 4D printing enables enhanced material properties, such as appropriate rheological properties, superior mechanical strength, improved thermal and electrical conductivity, tailored surface characteristics, and enhanced 4D effect performance. NPs also imbue smart materials with responsive behavior to multiple external stimuli, granting them the ability to adapt, reshape, self-heal, and more. Furthermore, through the incorporation of nanomaterials, 4D printing achieves remote actuation, intricate multistage shape transformations, and precise control over multiple stimuli, facilitating the versatile and efficient utilization of 4D printing in numerous intelligent structures and systems.

In the realm of biomedical applications, the potential of nanomaterials in 4D printing holds great promise for enhancing the capabilities of printed constructs. One future direction is the development of bioactive nanomaterial that can be incorporated into 4D-printed scaffolds for tissue engineering. These nanomaterials can provide enhanced cellular interactions, promote tissue regeneration, and offer a controlled release of bioactive molecules. This approach exhibits huge potential to reshape regenerative medicine by enabling the creation of functional and biocompatible tissue constructs. Another promising direction is the use of nanomaterials in 4D printing for drug delivery systems. By incorporating NPs with specific properties, such as controlled release capabilities or targeted drug delivery, 4D-printed structures can be designed to precisely release therapeutic agents in response to specific stimuli or physiological conditions. This opens up possibilities for personalized medicine and improved treatment efficacy. Moreover, nanomaterials integrated into 4D printing can enhance the mechanical properties and stability of biomedical devices, such as implants or prosthetics. By reinforcing 4D printed structures with nanomaterials, they can exhibit improved strength, durability, and biocompatibility.

In the domain of intelligent devices, one future direction involves the integration of nanomaterials with responsive polymers, enabling the creation of smart materials with tailored properties. These materials can exhibit SMEs, self-healing capabilities, and responsiveness to external stimuli, enabling the creation of intelligent devices that can adapt, change shape, or self-repair. Besides, the utilization of nanomaterials to enhance the sensing and actuation capabilities of 4D-printed intelligent devices is one of the promising future directions. By introducing NPs with specific properties, such as enhanced conductivity or sensitivity to environmental changes, 4D printed devices can be designed to detect and respond to various stimuli, enabling applications in fields like robotics, electronics, and energy harvesting. Additionally, nanomaterials integrated into 4D printing can enhance the mechanical strength, thermal conductivity, and electrical properties of intelligent devices. By reinforcing 4D printed structures with nanomaterials, devices can exhibit improved performance, durability, and efficiency.

In the aerospace industry, the future development of 4D printing mainly focuses on the following aspects. The incorporation of nanomaterials can improve the mechanical properties of 4D-printed aerospace components. By integrating NPs with high strength and stiffness, the resulting 4D-printed structures can exhibit improved durability, lightweight characteristics, and resistance to extreme conditions. This enables the development of more robust and efficient aerospace components, leading to enhanced performance and fuel efficiency. Moreover, the utilization of nanomaterials to improve thermal management in aerospace systems is also a significant future direction. Through the integration of nanomaterials possessing elevated thermal conductivity, 4D printed constructions can proficiently disperse heat, thereby reducing thermal strain and bolstering the overall dependability of aerospace equipment. Last but not least, the integration of nanomaterials in 4D printing enables the fabrication of intelligent aerospace components. By incorporating NPs with sensing capabilities, 4D-printed structures can monitor and

Figure 10. Nanomaterials serving for multi-functionalities. a–j) 4D printed SMMF that is able to swim through the complex maze under the stimuli of bubble, MF, and pH. a) Schematic of the 4D printed SMMF passing through the micromaze. b) Optical picture of the maze on a micro-scale. c–f) Under different pH environments, the fins of SMMF undergo shape morphing. When the pH is greater than 9, the opened fins do not allow the SMMF to pass through the microgap. However, when the pH is less than 9, the closed fins allow the SMMF to pass through the microgap. g,h) Opening (g) and closing (h) modes of SMMF at the start and finish point of micromaze, respectively. i) Sequential pictures of 4D-printed SMMF through the micromaze actuated by bubbles and MF. Panels a–i are reprinted with permission.[265] Copyright 1999–2023, John Wiley & Sons. j–l) 4D printed SMMC and SMMF serving for smart gripper and drug delivery respectively. j) Magnetic and pH-controlled cargo transportation process finished by 4D printed SMMC. k,l) Magnetic and pH-controlled drug delivery process finished by 4D printed SMMF. k) Schematic of *in vitro* drug delivery process finished by 4D printed SMMF. l) Viability of Hela cells in proximity to SMMF, with DOX and an opened mouth/ without DOX and an opened mouth/ with DOX and closed mouth. Panels j–l are reprinted with permission.[270] Copyright 2023, American Chemical Society. m) Schematic of silica NPs serving as nucleation sites in polymer matrix, promoting polymerization by reducing light scattering. Panels m is reprinted with permission.[145] Copyright 2023, Elsevier B.V. n,o) 4D printed growth factor releasing nerve conduits. n) Schematic showing composite 4D ink containing 4-HBA, PU-EO-PO monomer, initiator, and NCs used to print nerve conduit via DLP technology. o) Schematic of high-frequency MF-actuated NGF release and electric stimulation to promote guided nerve regeneration. Panels n,o are reprinted with permission.[266] Copyright 2023, Springer Nature.

respond to environmental changes, facilitating real-time feedback and adaptive functionalities in aerospace systems.

Although there are numerous opportunities in the realm of 4D printing, there are also many challenges that need to be addressed. 1) Material selection: Even though the introduction of nanomaterial is able to enhance the properties of 4D materials, choosing materials that can change shape as desired, endure multiple transformations, and respond predictably to external factors is a critical challenge. 2) Printing precision: Achieving high precision in 4D is crucial. Compared with extrusion-based printing technology, light-assisted print has a significantly higher resolution, and the photocurable requirement of the resin limits its application. Also, although some printing techniques have extremely high precision, for example, TPP, the high price limits their popularization. 3) Control, modeling, simulation, and predictability: Designing objects to transform as intended and accurately predicting their behavior are complex. Ensuring precise control of the transformation process and alignment with the intended final shape remains an ongoing challenge. 4) Stimulus responsiveness: crucially, the printed objects must respond correctly to external stimuli. Incorrect timing or inconsistency could result in unreliable or unintended transformations. 5) Scaling Up: While significant progress has been made in the laboratory setting, scaling up 4D printing for commercial or industrial applications introduces challenges related to production speed, consistency, and cost-effectiveness.

While the advancements in 4D printing research are captivating and hold great promise, the practical implementation and widespread application of 4D printing still lag behind. There is a considerable journey ahead to achieve full-scale industrialization in this field. In this context, the continued in-depth research on nanomaterials has provided an innovative and promising strategy to accelerate the application of 4D printing across diverse domains. There is a strong belief that the substantial demand for 4D printing will lead to significant breakthroughs in theory and technology. 4D printing and nanotechnology are expected to emerge as prominent technologies, presenting their practical value across diverse fields.

Acknowledgements

The authors would like to thank the financial support provided by NSF EBMS program Grants 1856321 and 2110842.

Conflict of Interest

The authors declare no conflict of interest.

Keywords

4D Printing, nanocomposites, nanomaterials, shape memory materials

Received: September 5, 2023
Revised: February 15, 2024
Published online:

[1] A. Su, S. J. Al'Aref, *3D Printing Applications in Cardiovascular Medicine* (Eds: S. J. Al'Aref, B. Mosadegh, S. Dunham, J. K. Min), Academic Press, Boston **2018**, p. 1.
[2] J.-Y. Lee, J. An, C. K. Chua, *Appl. Mater. Today* **2017**, *7*, 120.
[3] C. W. Hull, US4575330A, **1984**.
[4] S. Tibbits, presented at *The Emergence of "4D Printing"*, TED Talk, Long Beach, California, February **2013**.
[5] H. S. Atamian, N. M. Creux, R. I. Brown, A. G. Garner, B. K. Blackman, S. L. Harmer, *Science* **2016**, *353*, 587.
[6] M. C. Serrano, G. A. Ameer, *Macromol. Biosci.* **2012**, *12*, 1156.
[7] A. Melocchi, M. Uboldi, N. Inverardi, F. Briatico-Vangosa, F. Baldi, S. Pandini, G. Scalet, F. Auricchio, M. Cerea, A. Foppoli, A. Maroni, L. Zema, A. Gazzaniga, *Int. J. Pharm.* **2019**, *571*, 118700.
[8] R. L. Truby, M. Wehner, A. K. Grosskopf, D. M. Vogt, S. G. M. Uzel, R. J. Wood, J. A. Lewis, *Adv. Mater.* **2018**, *30*, 1706383.
[9] A. R. Rajkumar, K. Shanmugam, *J. Mater. Res.* **2018**, *33*, 4362.
[10] A. Haleem, M. Javaid, R. P. Singh, R. Suman, *Adv. Ind. Eng. Polym. Res.* **2021**, *4*, 301.
[11] Y. Kim, H. Yuk, R. Zhao, S. A. Chester, X. Zhao, *Nature* **2018**, *558*, 274.
[12] H. Cui, S. Miao, T. Esworthy, S.-J. Lee, X. Zhou, S. Y. Hann, T. J. Webster, B. T. Harris, L. G. Zhang, *Nano Res.* **2019**, *12*, 1381.
[13] Y. Wang, X. Li, *Composites, Part B* **2021**, *219*, 108918.
[14] A. M. Rosales, S. L. Vega, F. W. DelRio, J. A. Burdick, K. S. Anseth, *Angew. Chem., Int. Ed.* **2017**, *56*, 12132.
[15] S. B. Gugulothu, K. Chatterjee, *ACS Macro Lett.* **2023**, *12*, 494.
[16] H. Louro, A. Bettencourt, L. M. Gonçalves, A. J. Almeida, M. J. Silva, in *Nanotechnology Applications for Tissue Engineering* (Eds: S. Thomas, Y. Grohens, N. Ninan), William Andrew Publishing, Oxford **2015**, p. 263.
[17] L. R. Adil, R. Parui, M. N. Khatun, M. A. Chanu, L. Li, S. Wang, P. K. Iyer, in *Advanced Nanomaterials for Point of Care Diagnosis and Therapy* (Eds: S. Dave, J. Das, S. Ghosh), Elsevier, Amsterdam **2022**, p. 121.
[18] N. Joudeh, D. Linke, *J. Nanobiotechnol.* **2022**, *20*, 262.
[19] T. K. Sau, A. L. Rogach, F. Jäckel, T. A. Klar, J. Feldmann, *Adv. Mater.* **2010**, *22*, 1805.
[20] M. Hu, J. Chen, Z.-Y. Li, L. Au, G. V. Hartland, X. Li, M. Marquez, Y. Xia, *Chem. Soc. Rev.* **2006**, *35*, 1084.
[21] N. Khlebtsov, L. Dykman, *Chem. Soc. Rev.* **2011**, *40*, 1647.
[22] C. J. Murphy, A. M. Gole, J. W. Stone, P. N. Sisco, A. M. Alkilany, E. C. Goldsmith, S. C. Baxter, *Acc. Chem. Res.* **2008**, *41*, 1721.
[23] X. Li, J. Wang, L. Sun, Z. Wang, *Chem. Commun.* **2010**, *46*, 988.
[24] T. Lou, Y. Wang, J. Li, H. Peng, H. Xiong, L. Chen, *Anal. Bioanal. Chem.* **2011**, *401*, 333.
[25] C. L. Zavaleta, B. R. Smith, I. Walton, W. Doering, G. Davis, B. Shojaei, M. J. Natan, S. S. Gambhir, *Proc. Natl. Acad. Sci. USA* **2009**, *106*, 13511.
[26] S. S. Kumar, K. Kwak, D. Lee, *Anal. Chem.* **2011**, *83*, 3244.
[27] S. Lee, S.-M. Yoon, H.-J. Shin, W.-J. Joo, D. K. Yi, J.-Y. Choi, C. A. Amarnath, U. Paik, *Nanotechnology* **2008**, *19*, 075606.
[28] B. Van de Broek, N. Devoogdt, A. D'Hollander, H.-L. Gijs, K. Jans, L. Lagae, S. Muyldermans, G. Maes, G. Borghs, *ACS Nano* **2011**, *5*, 4319.
[29] Y. Wang, H. Cui, T. Esworthy, D. Mei, Y. Wang, L. G. Zhang, *Adv. Mater.* **2022**, *34*, 2109198.
[30] Y.-C. Sun, Y. Wan, R. Nam, M. Chu, H. E. Naguib, *Sci. Rep.* **2019**, *9*, 18754.
[31] T. Agarwal, S. Y. Hann, I. Chiesa, H. Cui, N. Celikkin, S. Micalizzi, A. Barbetta, M. Costantini, T. Esworthy, L. G. Zhang, C. De Maria, T. K. Maiti, *J. Mater. Chem. B* **2021**, *9*, 7608.
[32] H. Wang, J. Zhao, Z. Luo, Z. Li, *Magnetochemistry* **2023**, *9*, 204.

[33] I. A. 52900, *Additive manufacturing—General principles—Fundamentals and vocabulary*, ASTM International, Geneva, Switzerland **2021**.
[34] X. Wan, L. Luo, Y. Liu, J. Leng, *Adv. Sci.* **2020**, *7*, 2001000.
[35] V. G. Rocha, E. Saiz, I. S. Tirichenko, E. García-Tunon, *J. Mater. Chem. A* **2020**, *8*, 15646.
[36] P. K. Penumakala, J. Santo, A. Thomas, *Composites, Part B* **2020**, *201*, 108336.
[37] D. K. Yadav, R. Srivastava, S. Dev, *Mater. Today: Proc.* **2020**, *26*, 2089.
[38] H. H. Hamzah, S. A. Shafiee, A. Abdalla, B. A. Patel, *Electrochem. Commun.* **2018**, *96*, 27.
[39] A. Ahmed, S. Arya, V. Gupta, H. Furukawa, A. Khosla, *Polymer* **2021**, *228*, 123926.
[40] S. Y. Hann, H. Cui, T. Esworthy, S. Miao, X. Zhou, S.-J. Lee, J. P. Fisher, L. G. Zhang, *Transl. Res.* **2019**, *211*, 46.
[41] Q. Chen, L. Han, J. Ren, L. Rong, P. Cao, R. C. Advincula, *ACS Appl. Mater. Interfaces* **2020**, *12*, 50052.
[42] J. Liu, L. Zhao, Y. Guo, H. Zhang, Z. Zhang, *eXPRESS Polym. Lett.* **2020**, *14*, 348.
[43] G. Ehrmann, A. Ehrmann, *J. Appl. Polym. Sci.* **2021**, *138*, 50847.
[44] B. Tyler, D. Gullotti, A. Mangraviti, T. Utsuki, H. Brem, *Adv. Drug Delivery Rev.* **2016**, *107*, 163.
[45] J. Lai, X. Ye, J. Liu, C. Wang, J. Li, X. Wang, M. Ma, M. Wang, *Mater. Des.* **2021**, *205*, 109699.
[46] X. Wan, Y. He, Y. Liu, J. Leng, *Addit. Manuf.* **2022**, *53*, 102689.
[47] J. W. Boley, W. M. van Rees, C. Lissandrello, M. N. Horenstein, R. L. Truby, A. Kotikian, J. A. Lewis, L. Mahadevan, *Proc. Natl. Acad. Sci. USA* **2019**, *116*, 20856.
[48] B. Zhang, S. H. Chung, S. Barker, D. Craig, R. J. Narayan, J. Huang, *Prog. Nat. Sci.: Mater. Int.* **2021**, *31*, 180.
[49] A. Mitchell, U. Lafont, M. Holynska, C. Semprimoschnig, *Addit. Manuf.* **2018**, *24*, 606.
[50] H. Quan, T. Zhang, H. Xu, S. Luo, J. Nie, X. Zhu, *Bioact. Mater.* **2020**, *5*, 110.
[51] S. C. Ligon, R. Liska, J. Stampfl, M. Gurr, R. Mülhaupt, *Chem. Rev.* **2017**, *117*, 10212.
[52] J. Z. Manapat, Q. Chen, P. Ye, R. C. Advincula, *Macromol. Mater. Eng.* **2017**, *302*, 1600553.
[53] Y. Xu, Y. Zhu, Y. Sun, J. Jin, Y. Chen, *J. Manuf. Sci. Eng.* **2021**, *143*, 051008.
[54] H. Cui, C. Liu, T. Esworthy, Y. Huang, Z.-X. Yu, X. Zhou, H. San, S.-J. Lee, S. Y. Hann, M. Boehm, M. Mohiuddin, J. P. Fisher, L. G. Zhang, *Sci. Adv.* **2020**, *6*, abb5067.
[55] B. Zhang, A. Serjouei, Y.-F. Zhang, J. Wu, H. Li, D. Wang, H. Y. Low, Q. Ge, *Chem. Eng. J.* **2021**, *411*, 128466.
[56] J.-T. Miao, M. Ge, S. Peng, J. Zhong, Y. Li, Z. Weng, L. Wu, L. Zheng, *ACS Appl. Mater. Interfaces* **2019**, *11*, 40642.
[57] S. Miao, H. Cui, M. Nowicki, L. Xia, X. Zhou, S.-J. Lee, W. Zhu, K. Sarkar, Z. Zhang, L. G. Zhang, *Adv. Biosyst.* **2018**, *2*, 1800101.
[58] C. Zhang, X. Lu, G. Fei, Z. Wang, H. Xia, Y. Zhao, *ACS Appl. Mater. Interfaces* **2019**, *11*, 44774.
[59] C. Yuan, F. Wang, Q. Ge, *Extreme Mech. Lett.* **2021**, *42*, 101122.
[60] M. Nachimuthu, Rajesh P. K., *Rapid Prototyping J.* **2022**, *29*, 437.
[61] E. A. Clark, M. R. Alexander, D. J. Irvine, C. J. Roberts, M. J. Wallace, S. Sharpe, J. Yoo, R. J. M. Hague, C. J. Tuck, R. D. Wildman, *Int. J. Pharm.* **2017**, *529*, 523.
[62] C. Cui, D.-O. Kim, M. Y. Pack, B. Han, L. Han, Y. Sun, L.-H. Han, *Biofabrication* **2020**, *12*, 045018.
[63] X. Cui, D. Dean, Z. M. Ruggeri, T. Boland, *Biotechnol. Bioeng.* **2010**, *106*, 963.
[64] E. Tekin, P. J. Smith, U. S. Schubert, *Soft Matter* **2008**, *4*, 703.
[65] T. Agarwal, G. M. Fortunato, S. Y. Hann, B. Ayan, K. Y. Vajanthri, D. Presutti, H. Cui, A. H. P. Chan, M. Costantini, V. Onesto, C. Di Natale, N. F. Huang, P. Makvandi, M. Shabani, T. K. Maiti, L. G. Zhang, C. De Maria, *Mater. Sci. Eng., C* **2021**, *124*, 112057.
[66] H. Jia, S. Y. Gu, K. Chang, *Adv. Polym. Technol.* **2018**, *37*, 3222.
[67] C.-Y. Cheng, H. Xie, Z.-Y. Xu, L. Li, M.-N. Jiang, L. Tang, K.-K. Yang, Y.-Z. Wang, *Chem. Eng. J.* **2020**, *396*, 125242.
[68] D. Chen, Q. Liu, Z. Han, J. Zhang, H. Song, K. Wang, Z. Song, S. Wen, Y. Zhou, C. Yan, Y. Shi, *Adv. Sci.* **2020**, *7*, 2000584.
[69] C. Lin, J. Lv, Y. Li, F. Zhang, J. Li, Y. Liu, L. Liu, J. Leng, *Adv. Funct. Mater.* **2019**, *29*, 1906569.
[70] A. Basu, A. Saha, C. Goodman, R. T. Shafranek, A. Nelson, *ACS Appl. Mater. Interfaces* **2017**, *9*, 40898.
[71] C. Yuan, D. J. Roach, C. K. Dunn, Q. Mu, X. Kuang, C. M. Yakacki, T. J. Wang, K. Yu, H. J. Qi, *Soft Matter* **2017**, *13*, 5558.
[72] A. Li, A. Challapalli, G. Li, *Sci. Rep.* **2019**, *9*, 1.
[73] H. Wu, P. Chen, C. Yan, C. Cai, Y. Shi, *Mater. Des.* **2019**, *171*, 107704.
[74] D. Jin, Q. Chen, T.-Y. Huang, J. Huang, L. Zhang, H. Duan, *Materials Today* **2020**, *32*, 19.
[75] H. Zeng, P. Wasylczyk, C. Parmeggiani, D. Martella, M. Burresi, D. S. Wiersma, *Adv. Mater.* **2015**, *27*, 3883.
[76] Q. Ge, A. H. Sakhaei, H. Lee, C. K. Dunn, N. X. Fang, M. L. Dunn, *Sci. Rep.* **2016**, *6*, 31110.
[77] D. Han, Z. Lu, S. A. Chester, H. Lee, *Sci. Rep.* **2018**, *8*, 1963.
[78] D. Han, R. S. Morde, S. Mariani, A. A. La Mattina, E. Vignali, C. Yang, G. Barillaro, H. Lee, *Adv. Funct. Mater.* **2020**, *30*, 1909197.
[79] R. Wilhite, I. Wölfel, *Anat., Histol., Embryol.* **2019**, *48*, 609.
[80] Y. Shen, H. Tang, X. Huang, R. Hang, X. Zhang, Y. Wang, X. Yao, *Carbohydr. Polym.* **2020**, *235*, 115970.
[81] L. Yang, F. Mayer, U. H. F. Bunz, E. Blasco, M. Wegener, *Light: Adv. Manuf.* **2021**, *2*, 296.
[82] Y. Tao, L. Lin, X. Ren, X. Wang, X. Cao, H. Gu, Y. Ye, Y. Ren, Z. Zhang, *Micromachines* **2023**, *14*, 1656.
[83] E. Skliutas, D. Samsonasa, A. Čiburys, L. Kontenis, D. Gailevičius, J. Berzinš, D. Narbutis, V. Jukna, M. Vengris, S. Juodkazis, M. Malinauskas, *Virtual Phys. Prototyping* **2023**, *18*, 2228324.
[84] D. K. Limberg, J.-H. Kang, R. C. Hayward, *J. Am. Chem. Soc.* **2022**, *144*, 5226.
[85] A. Selimis, V. Mironov, M. Farsari, *Microelectron. Eng.* **2015**, *132*, 83.
[86] W. Chen, C. S. Fernandez, L. Xu, E. Velliou, S. Homer-Vanniasinkam, M. K Tiwari, in *3D Printing in Medicine* (Ed: D. M. Kalaskar), Woodhead Publishing, Cambridge **2023**, pp. 225–271.
[87] S. O'Halloran, A. Pandit, A. Heise, A. Kellett, *Adv. Sci.* **2023**, *10*, 2204072.
[88] W. Chu, Y. Tan, P. Wang, J. Xu, W. Li, J. Qi, Y. Cheng, *Adv. Mater. Technol.* **2018**, *3*, 1700396.
[89] Q. Ge, Z. Li, Z. Wang, K. Kowsari, W. Zhang, X. He, J. Zhou, N. X. Fang, *Int. J. Extreme Manuf.* **2020**, *2*, 022004.
[90] C. Sun, N. Fang, D. M. Wu, X. Zhang, *Sens. Actuators, A* **2005**, *121*, 113.
[91] S. Ushiba, S. Shoji, K. Masui, P. Kuray, J. Kono, S. Kawata, *Carbon* **2013**, *59*, 283.
[92] Y. Liu, W. Xiong, D. W. Li, Y. Lu, X. Huang, H. Liu, L. S. Fan, L. Jiang, J.-F. Silvain, Y. F. Lu, *Int. J. Extreme Manuf.* **2019**, *1*, 025001.
[93] D. Gonzalez-Hernandez, B. Sanchez-Padilla, D. Gailevicius, S. C. Thodika, S. Juodkazis, E. Brasselet, M. Malinauskas, *Adv. Opt. Mater.* **2023**, *11*, 2300258.
[94] Y.-L. Sun, W.-F. Dong, L.-G. Niu, T. Jiang, D.-X. Liu, L. Zhang, Y.-S. Wang, Q.-D. Chen, D.-P. Kim, H.-B. Sun, *Light: Sci. Appl.* **2014**, *3*, 129.
[95] S. Rekstyte, D. Paipulas, M. Malinauskas, V. Mizeikis, *Nanotechnology* **2017**, *28*, 124001.
[96] J. Qu, M. Kadic, A. Naber, M. Wegener, *Sci. Rep.* **2017**, *7*, 40643.
[97] H. Wei, Q. Zhang, Y. Yao, L. Liu, Y. Liu, J. Leng, *ACS Appl. Mater. Interfaces* **2017**, *9*, 876.
[98] Y. Wang, X. Li, *Composites, Part B* **2021**, *211*, 108644.

[99] W. Zhou, Z. Qiao, E. Nazarzadeh Zare, J. Huang, X. Zheng, X. Sun, M. Shao, H. Wang, X. Wang, D. Chen, J. Zheng, S. Fang, Y. M. Li, X. Zhang, L. Yang, P. Makvandi, A. Wu, *J. Med. Chem.* **2020**, *63*, 8003.
[100] N. Ashammakhi, O. Kaarela, *J. Craniofacial Surg.* **2017**, *28*, 1647.
[101] S. Y. Hann, H. Cui, M. Nowicki, L. G. Zhang, *Addit. Manuf.* **2020**, *36*, 101567.
[102] P. D. C. Costa, D. C. S. Costa, T. R. Correia, V. M. Gaspar, J. F. Mano, *Adv. Mater. Technol.* **2021**, *6*, 2100168.
[103] A. Belmonte, X. Fernández-Francos, S. De la Flor, *J. Mater. Sci.* **2017**, *52*, 1625.
[104] A. Yadav, S. K. Singh, S. Das, S. Kumar, A. Kumar, *Smart Mater. Struct.* **2023**, *32*, 095016.
[105] S. Thakur, J. Hu, in *Aspects of Polyurethanes* (Ed: F. Yilmaz), IntechOpen, Rijeka, Croatia **2017**, p. 53–71.
[106] S. K. Leist, D. Gao, R. Chiou, J. Zhou, *Virtual Phys. Prototyping* **2017**, *12*, 290.
[107] S. Miao, W. Zhu, N. J. Castro, M. Nowicki, X. Zhou, H. Cui, J. P. Fisher, L. G. Zhang, *Sci. Rep.* **2016**, *6*, 27226.
[108] J. Cui, F. R. Poblete, Y. Zhu, *Adv. Funct. Mater.* **2018**, *28*, 1802768.
[109] L. Zhou, Q. Liu, X. Lv, L. Gao, S. Fang, H. Yu, *J. Mater. Chem. C* **2016**, *4*, 9993.
[110] A. Cortés, A. Cosola, M. Sangermano, M. Campo, S. González Prolongo, C. F. Pirri, A. Jiménez-Suárez, A. Chiappone, *Adv. Funct. Mater.* **2021**, *31*, 2106774.
[111] F. Zhang, Y. Xia, L. Wang, L. Liu, Y. Liu, J. Leng, *ACS Appl. Mater. Interfaces* **2018**, *10*, 35526.
[112] L.-H. Shao, B. Zhao, Q. Zhang, Y. Xing, K. Zhang, *Extreme Mech. Lett.* **2020**, *39*, 100793.
[113] C. Feng, C. P. Hemantha Rajapaksha, J. M. Cedillo, C. Piedrahita, J. Cao, V. Kaphle, B. Lüssem, T. Kyu, A. Jákli, *Macromol. Rapid Commun.* **2019**, *40*, 1900299.
[114] X.-J. Han, Z.-Q. Dong, M.-M. Fan, Y. Liu, J.-H. li, Y.-F. Wang, Q.-J. Yuan, B.-J. Li, S. Zhang, *Macromol. Rapid Commun.* **2012**, *33*, 1055.
[115] A. Sydney Gladman, E. A. Matsumoto, R. G. Nuzzo, L. Mahadevan, J. A. Lewis, *Nat. Mater.* **2016**, *15*, 413.
[116] Z. Zhao, J. Wu, X. Mu, H. Chen, H. J. Qi, D. Fang, *Macromol. Rapid Commun.* **2017**, *38*, 1600625.
[117] H. Z. Lu, C. Yang, X. Luo, H. W. Ma, B. Song, Y. Y. Li, L. C. Zhang, *Mater. Sci. Eng., A* **2019**, *763*, 138166.
[118] A. Lai, Z. Du, C. L. Gan, C. A. Schuh, *Science* **2013**, *341*, 1505.
[119] K. Chen, X. Kuang, V. Li, G. Kang, H. J. Qi, *Soft Matter* **2018**, *14*, 1879.
[120] S. J. D. Lugger, L. Ceamanos, D. J. Mulder, C. Sánchez-Somolinos, A. P. H. J. Schenning, *Adv. Mater. Technol.* **2023**, *8*, 2201472.
[121] Y. Cheng, K. H. Chan, X.-Q. Wang, T. Ding, T. Li, X. Lu, G. W. Ho, *ACS Nano* **2019**, *13*, 13176.
[122] G. Gerstein, C. Kahra, O. Golovko, F. Schäfke, C. Klose, S. Herbst, F. Nürnberger, H. J. Maier, *Prod. Eng.* **2021**, *15*, 271.
[123] A. N. Alagha, S. Hussain, W. Zaki, *Mater. Des.* **2021**, *204*, 109654.
[124] M. P. Caputo, A. E. Berkowitz, A. Armstrong, P. Müllner, C. V. Solomon, *Addit. Manuf.* **2018**, *21*, 579.
[125] X. Kuang, D. J. Roach, J. Wu, C. M. Hamel, Z. Ding, T. Wang, M. L. Dunn, H. J. Qi, *Adv. Funct. Mater.* **2019**, *29*, 1805290.
[126] D.-G. Shin, T.-H. Kim, D.-E. Kim, *Int. J. Precis. Eng. Manuf.-Green Technol.* **2017**, *4*, 349.
[127] W. Zhu, T. J. Webster, L. G. Zhang, *Future Med.* **2019**, *14*, 1643.
[128] M. Das, R. S. Ambekar, S. K. Panda, S. Chakraborty, C. S. Tiwary, *J. Mater. Res.* **2021**, *36*, 4024.
[129] C. J. Hansen, in *3D and 4D Printing of Polymer Nanocomposite Materials* (Eds: K. Sadasivuni, K. Deshmukh, M. A. Almaadeed), Elsevier, Amsterdam **2020**, pp. 25–44.
[130] W. G. Kreyling, M. Semmler-Behnke, Q. Chaudhry, *Nano Today* **2010**, *5*, 165.
[131] J. Jeevanandam, A. Barhoum, Y. S. Chan, A. Dufresne, M. K. Danquah, *Beilstein J. Nanotechnol.* **2018**, *9*, 1050.
[132] E. Roduner, *Chem. Soc. Rev.* **2006**, *35*, 583.
[133] M. Alsaadi, E. P. Hinchy, C. T. McCarthy, V. F. Moritz, S. Zhuo, E. Fuenmayor, D. M. Devine, *J. Manuf. Mater. Process.* **2023**, *7*, 35.
[134] I. A. Rousseau, T. Xie, *J. Mater. Chem.* **2010**, *20*, 3431.
[135] S. Miao, H. Cui, T. Esworthy, B. Mahadik, S.-J. Lee, X. Zhou, S. Y. Hann, J. P. Fisher, L. G. Zhang, *Adv. Sci.* **2020**, *7*, 1902403.
[136] M. A. S. R. Saadi, A. Maguire, N. T. Pottackal, M.d S. H. Thakur, M. M.d. Ikram, A. J. Hart, P. M. Ajayan, M. M. Rahman, *Adv. Mater.* **2022**, *34*, 2108855.
[137] J. A. Lewis, *Adv. Funct. Mater.* **2006**, *16*, 2193.
[138] D. Therriault, S. R. White, J. A. Lewis, *Appl. Rheol.* **2007**, *17*, 10112.
[139] Z. Hou, H. Lu, Y. Li, L. Yang, Y. Gao, *Front. Mater.* **2021**, *8*, 647229.
[140] M. A. S. R. Saadi, A. Maguire, N. T. Pottackal, Md S. H. Thakur, M. Md. Ikram, A. John Hart, P. M. Ajayan, M. M. Rahman, *Adv. Mater.* **2022**, *34*, 2108855.
[141] Z. Chen, D. Zhao, B. Liu, G. Nian, X. Li, J. Yin, S. Qu, W. Yang, *Adv. Funct. Mater.* **2019**, *29*, 20, 1900971.
[142] M. Falahati, P. Ahmadvand, S. Safaee, Y.-C. Chang, Z. Lyu, R. Chen, L. Li, Y. Lin, *Mater. Today* **2020**, *40*, 215.
[143] M. C. Li, Q. Wu, R. J. Moon, M. A. Hubbe, M. J. Bortner, *Adv. Mater.* **2021**, *33*, 21, 2006052.
[144] C. Yadav, A. Saini, W. Zhang, X. You, I. Chauhan, P. Mohanty, X. Li, *Int. J. Biol. Macromol.* **2021**, *166*, 1586.
[145] Y. Y. C. Choong, S. Maleksaeedi, H. Eng, S. Yu, J. Wei, P.-C. Su, *Appl. Mater. Today* **2020**, *18*, 100515.
[146] Q. Chen, T. Sukmanee, L. Rong, M. Yang, J. Ren, S. Ekgasit, R. Advincula, *ACS Appl. Polym. Mater.* **2020**, *2*, 5492.
[147] J.-W. Su, W. Gao, K. Trinh, S. M. Kenderes, E. Tekin Pulatsu, C. Zhang, A. Whittington, M. Lin, J. Lin, *Int. J. Smart Nano Mater.* **2019**, *10*, 237.
[148] X. Kuang, K. Chen, C. K. Dunn, J. Wu, V. C. F. Li, H. J. Qi, *ACS Appl. Mater. Interfaces* **2018**, *10*, 8, 7381.
[149] X. Li, Y. Yang, Y. Zhang, T. Wang, Z. Yang, Q. Wang, X. Zhang, *Mater. Des.* **2020**, *191*, 108606.
[150] H. Chi, Z. Lin, Y. Chen, R. Zheng, H. Qiu, X. Hu, H. Bai, *ACS Appl. Mater. Interfaces* **2022**, *14*, 11, 13758.
[151] G. Cheraghian, M. P. Wistuba, *Nanomaterials (Basel)* **2021**, *11*, 454.
[152] G. D. Shay, *Thickeners and Rheology Modifiers*, in: J. V. Koleske (Ed.), 14th ed., ASTM International, PA, USA 1995, **1995** 268 (Chapter 30).
[153] H. Barthel, L. Rösch, J. Weis, in *Organosilicon Chemistry Set: From Molecules to Materials* (Eds: N. Auner, J. Weis), Weinheim, Germany **2005**, p. 761–778.
[154] P. D. A. Bode, *Informatik-Spektrum* **2006**, *29*, 1.
[155] H. A. Barnes, *J. Non-Newtonian Fluid Mech.* **1997**, *70*, 1.
[156] H. Barthel, M. Dreyer, T. Gottschalk-Gaudig, V. Litvinov, E. Nikitina, *Macromol. Symp.* **2002**, *187*, 573.
[157] Ç. Kırbıyık Kurukavak, *Reference Module in Materials Science and Materials Engineering*, Elsevier, Amsterdam **2022**.
[158] C. N. R. Rao, K. Biswas, K. S. Subrahmanyam, A. Govindaraj, *J. Mater. Chem.* **2009**, *19*, 2457.
[159] A. Bakak, M. Lotfi, R. Heyd, A. Ammar, A. Koumina, *Entropy* **2021**, *23*, 979.
[160] K. S. Vasu, R. Krishnaswamy, S. Sampath, A. K. Sood, *Soft Matter* **2013**, *9*, 5874.
[161] A. Carnicer-Lombarte, D. G. Barone, I. B. Dimov, R. S. Hamilton, M. Prater, X. Zhao, A. L. Rutz, *Biorxiv* **2019**, 829648.
[162] A. Carnicer-Lombarte, S.-T. Chen, G. G. Malliaras, D. G. Barone, *Front. Bioeng. Biotechnol.* **2021**, 271.
[163] S. Roy, J. Ryan, S. Webster, D. Nepal, *Appl. Mech. Rev.* **2017**, *69*, 050802.
[164] D. G. Papageorgiou, Z. Li, M. Liu, I. A. Kinloch, R. J. Young, *Nanoscale* **2020**, *12*, 2228.
[165] A. J. Crosby, J. Y. Lee, *Polym. Rev.* **2007**, *47*, 217.
[166] E. Kontou, A. Christopoulos, P. Koralli, D. E. Mouzakis, *Nanomaterials* **2023**, *13*, 1095.

[167] F. Ondreas, P. Lepcio, M. Zboncak, K. Zarybnicka, L. E. Govaert, J. Jancar, *Macromolecules* **2019**, *52*, 6250.
[168] J. Zaragoza, S. Fukuoka, M. Kraus, J. Thomin, P. Asuri, *Nanomaterials* **2018**, *8*, 882.
[169] S. Cheng, V. Bocharova, A. Belianinov, S. Xiong, A. Kisliuk, S. Somnath, A. P. Holt, O. S. Ovchinnikova, S. Jesse, H. Martin, T. Etampawala, M. Dadmun, A. P. Sokolov, *Nano Lett.* **2016**, *16*, 3630.
[170] R. Sun, M. Melton, N. Safaie, R. C. Ferrier, S. Cheng, Y. Liu, X. Zuo, Y. Wang, *Phys. Rev. Lett.* **2021**, *126*, 117801.
[171] U. De Maio, N. Fantuzzi, F. Greco, L. Leonetti, A. Pranno, *Nanomaterials* **2020**, *10*, 1792.
[172] M. N. Niyaraki, J. Mirzaei, H. Taghipoor, *Polym. Bull.* **2022**, *80*, 9507.
[173] E. Y. Lin, A. L. Frischknecht, R. A. Riggleman, *Macromolecules* **2020**, *53*, 2976.
[174] J. Shen, X. Lin, J. Liu, X. Li, *Phys. Chem. Chem. Phys.* **2020**, *22*, 16760.
[175] A. Idowu, T. Thomas, B. Boesl, A. Agarwal, *J. Manuf. Sci. Eng.* **2023**, *145*, 4, 041003.
[176] Y. Zhou, F. Wang, Z. Yang, X. Hu, Y. Pan, Y. Lu, M. Jiang, *Ind. Crops Prod.* **2022**, *182*, 114831.
[177] T. Gu, H. Bi, H. Sun, J. Tang, Z. Ren, X. Zhou, M. Xu, *Addit. Manuf.* **2023**, *70*, 103544.
[178] J. Wang, F. Song, Y. Ding, M. Shao, *Mater. Des.* **2020**, *195*, 109073.
[179] C. Si, Z. Sun, F. Liu, *Nanoscale* **2016**, *8*, 3207.
[180] G. Yang, L. Li, W. B. Lee, M. C. Ng, *Sci. Technol. Adv. Mater.* **2018**, *19*, 613.
[181] J. R. Potts, D. R. Dreyer, C. W. Bielawski, R. S. Ruoff, *Polymer* **2011**, *52*, 5.
[182] A. Kumar, K. Sharma, A. R. Dixit, *Carbon Lett.* **2021**, *31*, 149.
[183] Y. Wang, Z. Li, J. Wang, J. Li, Y. Lin, *Trends Biotechnol.* **2011**, *29*, 205.
[184] E. Casero, A. M. Parra-Alfambra, M. D. Petit-Domínguez, F. Pariente, E. Lorenzo, C. Alonso, *Electrochem. Commun.* **2012**, *20*, 63.
[185] J. Chowdhury, P. V. Anirudh, C. Karunakaran, V. Rajmohan, A. T. Mathew, K. Koziol, W. F. Alsanie, C. Kannan, A. S. S. Balan, V. K. Thakur, *Polymers* **2021**, *13*, 3660.
[186] M. Jonoobi, R. Oladi, Y. Davoudpour, K. Oksman, A. Dufresne, Y. Hamzeh, R. Davoodi, *Cellulose* **2015**, *22*, 935.
[187] D. A. Gopakumar, S. Thomas, Y. Grohens, in *Multifunctional Polymeric Nanocomposites Based on Cellulosic Reinforcements* (Eds: D. Puglia, E. Fortunati, J. M. Kenny), William Andrew Publishing, Norwich, NY, USA **2016**, pp. 253–275.
[188] V. Barbash, O. Yashchenko, A. Kedrovska, *J. Sci. Res. Rep.* **2017**, *16*, 1.
[189] J. Luo, H. Chang, A. A. Bakhtiary Davijani, H. Clive Liu, P.-H. Wang, R. J. Moon, S. Kumar, *Cellulose* **2017**, *24*, 1745.
[190] C. Guise, R. Fangueiro, in *Natural Fibres: Advances in Science and Technology Towards Industrial Applications* (Eds: R. Fangueiro, S. Rana), Springer, Dordrecht **2016**, pp. 155–169.
[191] H. Bi, Z. Ren, G. Ye, H. Sun, R. Guo, X. Jia, M. Xu, *Cellulose* **2020**, *27*, 8011.
[192] D. Tian, F. Wang, Z. Yang, X. Niu, Q. Wu, P. Sun, *Carbohydr. Polym.* **2019**, *219*, 191.
[193] H. Kargarzadeh, A. Galeski, A. Pawlak, *Polymer* **2020**, *203*, 122748.
[194] M. Barmouz, A. H. Behravesh, *Composites, Part A* **2017**, *101*, 160.
[195] M. Behl, A. Lendlein, *Mater. Today* **2007**, *10*, 20.
[196] T. S. Hebner, M. Podgórski, S. Mavila, T. J. White, C. N. Bowman, *Angew. Chem., Int. Ed.* **2022**, *61*, 202116522.
[197] H. Yang, W. R. Leow, T. Wang, J. Wang, J. Yu, K. He, D. Qi, C. Wan, X. Chen, *Adv. Mater.* **2017**, *29*, 1701627.
[198] W. Wagermaier, K. Kratz, M. Heuchel, A. Lendlein, in *Shape-Memory Polymers* (Ed: A. Lendlein), Springer, Berlin, Heidelberg **2010**, pp. 97–145.
[199] Y. Hu, Z. Li, T. Lan, W. Chen, *Adv. Mater.* **2016**, *28*, 10548.
[200] R. Tang, Z. Liu, D. Xu, J. Liu, L. Yu, H. Yu, *ACS Appl. Mater. Interfaces* **2015**, *7*, 16, 8393.
[201] H. Y. Jiang, S. Kelch, A. Lendlein, *Adv. Mater.* **2006**, *18*, 1471.
[202] Y.u Wang, E. Sachyani Keneth, A. Kamyshny, G. Scalet, F. Auricchio, S. Magdassi, *Adv. Mater. Technol.* **2022**, *7*, 2101058.
[203] A. Nishiguchi, H. Zhang, S. Schweizerhof, M. F. Schulte, A. Mourran, M. Mo̎ller, *ACS Appl. Mater. Interfaces* **2020**, *12*, 10, 12176.
[204] V. Vitola, I. Bite, I. Apsite, A. Zolotarjovs, A. Biswas, *J. Polym. Res.* **2021**, *28*, 13.
[205] Y. Wang, H. Cui, Y. Wang, C. Xu, T. J. Esworthy, S. Y. Hann, M. Boehm, Y.-L. Shen, D. Mei, L. G. Zhang, *ACS Appl. Mater. Interfaces* **2021**, *13*, 11, 12746.
[206] J. Gong, P. Cao, J. Yang, Z. Tang, X. Zhang, Q. Wang, T. Wang, X. Pei, Y. Zhang, *Macromol. Mater. Eng.* **2022**, *307*, 2200354.
[207] H. Bi, G. Ye, H. Yang, H. Sun, Z. Ren, R. Guo, M. Xu, L. Cai, Z. Huang, *Eur. Polym. J.* **2020**, *136*, 109920.
[208] Z. Tang, D. Ma, Q. Chen, Y. Wang, M. Sun, Q. Lian, J. Shang, P. K. Wong, C. He, D. Xia, T. Wang, *J. Hazard. Mater.* **2022**, *437*, 129373.
[209] S. Loeb, C. Li, J.-H. Kim, *Environ. Sci. Technol.* **2018**, *52*, 205.
[210] X. Cui, Q. Ruan, X. Zhuo, X. Xia, J. Hu, R. Fu, Y. Li, J. Wang, H. Xu, *Chem. Rev.* **2023**, *123*, 6891.
[211] P. Cheng, D. Wang, P. Schaaf, *Adv. Sustainable Syst.* **2022**, *6*, 2200115.
[212] J. Zeng, D. Goldfeld, Y. Xia, *Angew. Chem., Int. Ed.* **2013**, *52*, 4169.
[213] L. Xiao, X. Chen, X. Yang, J. Sun, J. Geng, *ACS Appl. Polym. Mater.* **2020**, *2*, 4273.
[214] H. Chen, L. Shao, T. Ming, Z. Sun, C. Zhao, B. Yang, J. Wang, *Small* **2010**, *6*, 2272.
[215] *Nanoparticle Technology Handbook*, (Eds: M. Hosokawa, K. Nogi, M. Naito, T. Yokoyama), Elsevier, Amsterdam **2008**, pp. 593–596.
[216] G. H. Woehrle, L. O. Brown, J. E. Hutchison, *J. Am. Chem. Soc.* **2005**, *127*, 2172.
[217] J. Song, P. Huang, X. Chen, *Nat. Protoc.* **2016**, *11*, 2287.
[218] K. K. Bharadwaj, B. Rabha, S. Pati, T. Sarkar, B. K. Choudhury, A. Barman, D. Bhattacharjya, A. Srivastava, D. Baishya, H. A. Edinur, Z. Abdul Kari, N. H. Mohd Noor, *Molecules* **2021**, *26*, 6389.
[219] X. Huang, M. A. El-Sayed, *J. Adv. Res.* **2010**, *1*, 13.
[220] R. Sardar, A. M. Funston, P. Mulvaney, R. W. Murray, *Langmuir* **2009**, *25*, 13840.
[221] X. Huang, S. Neretina, M. A. El-Sayed, *Adv. Mater.* **2009**, *21*, 4880.
[222] J. Zheng, X. Cheng, H. Zhang, X. Bai, R. Ai, L. Shao, J. Wang, *Chem. Rev.* **2021**, *121*, 13342.
[223] Y. Li, W. Lu, Q. Huang, C. Li, W. Chen, *Nanomedicine (Lond)* **2010**, *5*, 1161.
[224] Y.-T. Kwon, G.-D. Lim, S. Kim, S. H. Ryu, H.-R. Lim, Y.-H. Choa, *Appl. Surf. Sci.* **2019**, *477*, 204.
[225] L. Wang, *RSC Adv.* **2016**, *6*, 82596.
[226] W. Gao, Y. Sun, M. Cai, Y. Zhao, W. Cao, Z. Liu, G. Cui, B. Tang, *Nat. Commun.* **2018**, *9*, 231.
[227] S. Goel, F. Chen, W. Cai, *Small* **2014**, *10*, 631.
[228] D. Han, Y. Li, X. Liu, K. W. K. Yeung, Y. Zheng, Z. Cui, Y. Liang, *J. Mater. Sci. Technol.* **2021**, *62*, 83.
[229] Y. Cheng, S. Cheng, B. Chen, J. Jiang, C. Tu, W. Li, Y. Yang, K. Huang, K. Wang, H. Yuan, J. Li, Y. Qi, Z. Liu, *J. Am. Chem. Soc.* **2022**, *144*, 15562.
[230] J. Zhu, H. Zhang, F. Li, J. Liu, Y. Lin, *Appl. Phys. A* **2021**, *127*, 741.
[231] J.-L. Li, X.-L. Hou, H.-C. Bao, L. Sun, B. Tang, J.-F. Wang, X.-G. Wang, M. Gu, *J. Biomed. Mater. Res. A* **2014**, *102*, 2181.
[232] J. Wu, Z. Li, Y. Li, A. Pettitt, F. Zhou, *Technol. Cancer Res. Treat.* **2018**, *17*, 153303461876863.
[233] H. Dai, *Surf. Sci.* **2002**, *500*, 218.
[234] C. Zhang, L. Wu, M. de Perrot, X. Zhao, *Front. Oncol.* **2021**, *11*, 693814.
[235] M.-J. Wang, C. A. Gray, S. A. Reznek, K. Mahmud, Y. Kutsovsky, *Carbon Black*, in *Kirk-Othmer Encyclopedia of Chemical Technology*.
[236] M. E. Matter, L. Čamdžić, E. E. Stache, *Angew. Chem., Int. Ed.* **2023**, *62*, 202308648.

[237] D. Kim, J. Moon, *Electrochem. Solid-State Lett.* **2005**, *8*, J30.
[238] A. A. Bessonov, M. N. Kirikova, D. I. Petukhov, M. Allen, T. Ryhänen, M. J. A. Bailey, *Nat. Mater.* **2015**, *14*, 199.
[239] D. Li, W.-Y. Lai, Y.-Z. Zhang, W. Huang, *Adv. Mater.* **2018**, *30*, 1704738.
[240] A. Miriyev, K. Stack, H. Lipson, *Nat. Commun.* **2017**, *8*, 596.
[241] H. Deng, C. Zhang, K. Sattari, Y. Ling, J.-W. Su, Z. Yan, J. Lin, *ACS Appl. Mater. Interfaces* **2020**, *13*, 12719.
[242] J. Ahn, Y. Jeong, Z.-J. Zhao, S. Hwang, K. Kim, J. Ko, S. Jeon, *Adv. Mater. Technol.* **2019**, *5*, 2, 1900997.
[243] J. N. Rodriguez, C. Zhu, E. B. Duoss, T. S. Wilson, C. M. Spadaccini, J. P. Lewicki, *Sci. Rep.* **2016**, *6*, 27933.
[244] H. Wei, X. Cauchy, I. O. Navas, Y. Abderrafai, K. Chizari, U. Sundararaj, Y. Liu, J. Leng, D. Therriault, *ACS Appl. Mater. Interfaces* **2019**, *11*, 27, 24523.
[245] T. T. Nguyen, J. Kim, *Fibers Polym.* **2020**, *21*, 2364.
[246] Z. Yang, J. Tian, Z. Yin, C. Cui, W. Qian, F. Wei, *Carbon* **2019**, *141*, 467.
[247] T. M. Radadiya, *Eur. J. Mater. Sci.* **2015**, *2*, 6.
[248] A. Kausar, I. Ahmad, T. Zhao, O. Aldaghri, M. H. Eisa, *Processes* **2023**, *11*, 868.
[249] N. Hiremath, G. Bhat, in *Structure and Properties of High-Performance Fibers* (Ed: G. Bhat), Woodhead Publishing, Oxford **2017**, pp. 79–109.
[250] O. Pryshchepa, P. Pomastowski, B. Buszewski, *Adv. Colloid Interface Sci.* **2020**, *284*, 102246.
[251] T. Huang, X.-H. N. Xu, *J. Mater. Chem.* **2010**, *20*, 9867.
[252] A. Kamyshny, S. Magdassi, *Small* **2014**, *10*, 3515.
[253] P. Zhang, I. Wyman, J. Hu, S. Lin, Z. Zhong, Y. Tu, Z. Huang, Y. Wei, *Mater. Sci. Eng., B* **2017**, *223*, 1.
[254] Y. Yang, A. Chawla, J. Zhang, A. Esa, H. L. Jang, A. Khademhosseini, in *Principles of Regenerative Medicine*, 3rd ed. (Eds: A. Atala, R. Lanza, T. Mikos, R. Nerem), Academic Press, Boston **2019**, pp. 485–504.
[255] R. U. Hassan, S. Jo, J. Seok, *J. Appl. Polym. Sci.* **2018**, *135*, 45997.
[256] C. Wang, N. Chen, T. Yang, Q. Cheng, Y. Xiao, S. He, N. Song, *J. Magn. Magn. Mater.* **2023**, *565*, 170267.
[257] L. Hao, J. Li, P. Wang, Z. Wang, Z. Wu, Y. Wang, Z. Jiao, *Adv. Funct. Mater.* **2021**, *31*, 15, 2009661.
[258] M. D. Nguyen, H.-V. Tran, S. Xu, T. R. Lee, *Appl. Sci.* **2021**, *11*, 11301.
[259] D. Bobo, K. J. Robinson, J. Islam, K. J. Thurecht, S. R. Corrie, *Pharm. Res.* **2016**, *33*, 2373.
[260] Y. Gossuin, P. Gillis, A. Hocq, Q. L. Vuong, A. Roch, *Wiley Interdiscip. Rev.: Nanomed. Nanobiotechnol.* **2009**, *1*, 3, 299.
[261] R. A. Revia, M. Zhang, *Mater. Today* **2016**, *19*, 157.
[262] G. D. Soto, C. Meiorin, D. Actis, P. Mendoza Zélis, M. A. Mosiewicki, N. E. Marcovich, *Polym. Test.* **2018**, *65*, 360.
[263] C. Lin, L. Liu, Y. Liu, J. Leng, *ACS Appl. Mater. Interfaces* **2021**, *13*, 12668.
[264] S. Huang, M. Shan, H. Zhang, J. Sheng, J. Zhou, C. Cui, J. Wei, W. Zhu, J. Lu, *Polym.-Plast. Technol. Mater.* **2022**, *61*, 923.
[265] C. Xin, D. Jin, R. Li, D. Wang, Z. Ren, B. Liu, C. Chen, L. Li, S. Liu, B. Xu, Y. Zhang, Y. Hu, J. Li, L. Zhang, D. Wu, J. Chu, *Small* **2022**, *18*, 2202272.
[266] J.-H. Fang, H.-H. Hsu, R.-S. Hsu, C.-K. Peng, Y.-J. Lu, Y.-Y. Chen, S.-Y. Chen, S.-H. Hu, *NPG Asia Mater.* **2020**, *12*, 61.
[267] P. Phuhongsung, M. Zhang, S. Devahastin, A. S. Mujumdar, *Compr. Rev. Food Sci. Food Saf.* **2022**, *21*, 3455.
[268] X. Teng, M. Zhang, A. S. Mujumdar, *Trends Food Sci. Technol.* **2021**, *110*, 349.
[269] C. Shen, W. Chen, C. Li, X. Chen, H. Cui, L. Lin, *J. Food Eng.* **2023**, *342*, 111357.
[270] C. Xin, D. Jin, Y. Hu, L. Yang, R. Li, L. Wang, Z. Ren, D. Wang, S. Ji, K. Hu, D. Pan, H. Wu, W. Zhu, Z. Shen, Y. Wang, J. Li, L. Zhang, D. Wu, J. Chu, *ACS Nano* **2021**, *15*, 18048.

Shengbo Guo is a Ph.D. research scholar in the School of Engineering & Applied Science at George Washington University. He received his master's degree from New York University. His research interests include 3D/4D printing, tissue engineering, nanomaterials and their application in biomedical engineering.

Haitao Cui is currently a professor at the College of Bioengineering, Chongqing University. He conducted graduate research at Changchun Institute of Applied Chemistry, Chinese Academy of Science, and received his Ph.D. degree from the University of Chinese Academy of Sciences. From 2015 to 2022, he worked in Prof. Zhang's lab as a postdoc scientist and research scientist at The George Washington University. His research focuses on biomaterials and biomanufacturing technologies for tissue regeneration and disease studies.

Tarun Agarwal is a postdoctoral associate in the School of Engineering and Applied Science at George Washington University, Washington, D.C., USA. Previously, he served as an assistant professor at Koneru Lakshmaiah Education Foundation, Vijayawada, India (2022–2023). He received his Ph.D. degree from the Indian Institute of Technology, Kharagpur, India, in 2021. His research interests include biomaterials, 3D/4D printing, regenerative medicines, stem cell engineering, and lab-on-a-paper chips.

Lijie Grace Zhang is a professor and associate dean for research in the School of Engineering & Applied Science at George Washington University. She is also the director of the Bioengineering Laboratory for Nanomedicine and Tissue Engineering at GW. She received her Ph.D. in biomedical engineering at Brown University in 2009 and did her postdoctoral training at Rice University and Harvard Medical School. Her major research interests include 3D/4D printing, nanomaterials, complex tissue engineering, stem cell engineering, biorobots, and cancer metastasis models.